

Ferrocene-Functionalized Dithiocarbamate Zinc(II) Complexes as Efficient Bifunctional Catalysts for the One-Pot Synthesis of Chromene and Imidazopyrimidine Derivatives via Knoevenagel Condensation Reaction

Anamika, Chote Lal Yadav, Michael G. B. Drew, Kamlesh Kumar,* and Nanhai Singh*

Cite This: *Inorg. Chem.* 2021, 60, 6446–6462

Read Online

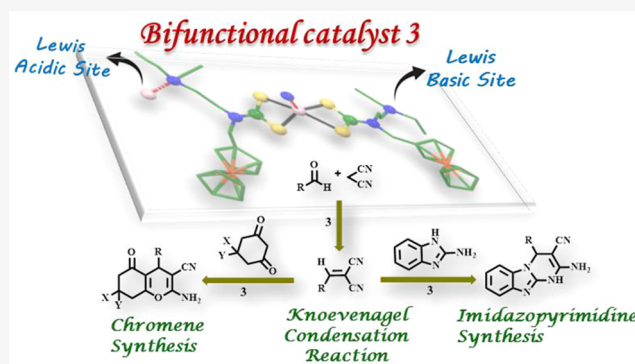
ACCESS |

Metrics & More

Article Recommendations

Supporting Information

ABSTRACT: Four new mononuclear/coordination polymeric (CP) zinc(II) complexes (1–4) of ferrocenyl/pyridyl-functionalized dithiocarbamate ligands, *N*-ferrocenylmethyl-*N*-butyl dithiocarbamate (L1), *N*-ferrocenylmethyl-*N*-ethylmorpholine dithiocarbamate (L2), *N*-ferrocenylmethyl-*N*-2-(diethylamino)ethylamine dithiocarbamate (L3), and *N*-4-methoxybenzyl-*N*-3-methylpyridyl dithiocarbamate (L4), have been synthesized and characterized by elemental analyses, IR, UV–vis, and ¹H and ¹³C{¹H} NMR spectroscopic techniques. The solid-state structures of complexes 1, 3, and 4 have been determined by single-crystal X-ray crystallography as well as powder X-ray diffraction. Single-crystal X-ray crystallography revealed a monomeric structure for complex 1 but 1D polymeric structures for complexes 3 and 4. In all complexes, dithiocarbamate ligands are bonded to the Zn(II) metal ion in a S²S chelating mode, and in the CPs, N atoms on the 2-(diethylamino)ethylamine and 3-pyridyl functionalities in the ligands on the neighboring molecules are also bonded to metal centers, leading to the formation of either a discrete tetrahedral molecule in 1 or 1D CP structures in 3 and 4. The Zn(II) metal centers in the polymeric structures exhibited either square-pyramidal or octahedral geometries. The supramolecular structures in these complexes are sustained via C–H⋯π (ZnCS₂, chelate; 3 and 4), C–H⋯π, and H⋯H interactions. The catalytic performances of complexes have also been assessed in the Knoevenagel condensation and one-pot multicomponent reactions. Catalysis results showed that the CP 3 acts as a heterogeneous bifunctional catalyst with excellent transformation efficiency at low catalyst loading.



INTRODUCTION

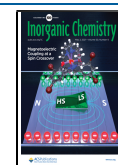
The Knoevenagel reaction, a well-known synthetic methodology for C–C bond formation by the condensation of aldehydes and active methylene compounds, has been extensively applied for the synthesis of important chemicals and pharmaceutical products.¹ Also, the products of Knoevenagel condensation are key intermediates in many one-pot multicomponent organic transformation reactions including the synthesis of 2-amino-4*H*-chromene and imidazopyrimidine derivatives. The chromene derivatives show several pharmacological properties including antitumor, antimalarial, anti-HIV, antimicrobial, antiinflammatory, and anti-allergenic.² Similarly, imidazopyrimidine derivatives exhibited a wide range of biological and pharmacological applications such as antimicrobial, antibacterial, antiinflammatory, antitubercular agents, anticancer, antimalarial, antihypertensive, antineoplastic, calcium antagonist,³ and CK2 inhibitor and are used for the treatment of anxiety disorders, ulcers, etc.⁴

Owing to the importance of these chromene and imidazopyrimidine derivatives in the pharmaceutical industry,

the development of an efficient catalytic system for the synthesis of these organic molecules that especially operates under mild reaction conditions is needed, so as to lower the energy consumption and also production costs. A variety of metal–organic framework (MOF) catalysts, such as zeolite imidazolate frameworks, many solid-supported amine-functionalized catalysts, heterometallic catalysts, cation-exchange zeolites, and ionic liquids, have been utilized for this reaction.⁵ Albeit there are only a few examples of heterogeneous bifunctional catalysts, based on coordination polymers (CPs) having both active sites, i.e., coordinatively unsaturated metal centers acting as the Lewis acidic sites and free Lewis basic sites within the same molecular framework.⁶ It has been shown

Received: January 18, 2021

Published: April 21, 2021



that such bifunctional catalytic systems exhibited enhanced catalytic activity in comparison to the monomeric complexes. The search for a rational design and synthesis of MOFs with suitable scaffolds for this reaction to produce efficient transformations is highly desirable. In addition, process chemists have been concerned with associated issues such as mild reaction conditions, green chemistry, low catalyst loading, recyclability and purity of products formed, and low cost with the use of catalysts.

There are certain reports that highlight the catalytic behavior of transition-metal-based MOFs/CPs as bifunctional catalysts toward the Knoevenagel condensation reaction as well as one-pot multicomponent reactions.⁶ The tandem one-pot deacetalization–Knoevenagel condensation reaction has been described using the PCN-124 MOF as a heterogeneous catalyst for the synthesis of benzylidene malononitrile where Cu(II) centers behaved as weak Lewis acidic sites while pyridine groups worked as Lewis basic sites.^{6a} Another Cu(II)/amine-based MOF (Cu₃TATAT) as a bifunctional catalyst has been employed for a one-pot aerobic oxidation/Knoevenagel condensation reaction in the absence of basic additives.^{6b} Han et al. reported two similar core–shell MOF@COFs (PCN-222-Co@TpPa-1 and UiO-66@SNW-1) as robust bifunctional catalysts for deacetalization–Knoevenagel cascade reactions.^{6c,d} Kim et al. have described the remarkable substrate selectivity shown by the bifunctional catalyst NH₂-MIL-101(Al) in the tandem Meinwald rearrangement–Knoevenagel condensation reaction.^{6e} Another Zr-based MOF, UiO-66-NH₂ with acidic (Zr) and basic (–NH₂) sites, gave 98% conversion of aldehyde to benzylidene malononitrile in the Knoevenagel condensation reaction.^{6f} Recently, some Zn(II) and Cd(II) MOF/CPs have also been investigated as bifunctional heterogeneous catalysts for such condensation reactions.^{5b,6i}

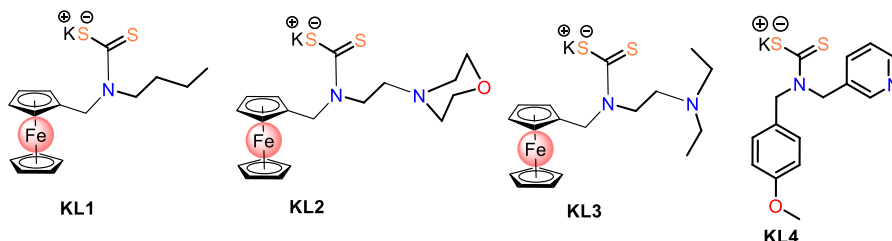
The metal thiolato complexes including dithiocarbamates have been used as catalysts for a variety of transformations.⁷ Our research group has developed several transition-metal complexes of functionalized thiolato ligand systems that afford systematically designed ordered architectures, and also these complexes have been used in catalysis for the synthesis of triazoles via Click reactions,^{7f–h} Chan–Lam coupling,⁷ⁱ electrocatalytic oxygen evolution,^{7e} etc. Most recently, we have turned our attention to investigate zinc(II)/cadmium(II) β -oxodithioester complexes in Knoevenagel reactions and one-pot multicomponent reactions.⁶ⁱ Within the realm of metal dithiolates, the dithiocarbamate ligands have occupied the first-row position because of their rich structural varieties, optical and conducting properties, and applications as sensitizers in solar energy schemes, single-source precursors for the preparation of metal sulfide thin films, rubber vulcanization accelerators, and medicines and in biological systems.⁸ Notwithstanding their synthetic versatility and practical utility, the catalytic activity of ubiquitous dithiocarbamate ligand complexes has not been investigated in this reaction until now. Encouraged by our recent study⁶ⁱ and in a continuation of our ongoing efforts, we were tempted to undertake the synthesis and crystal structures of new ferrocenyl/pyridyl-functionalized dithiocarbamate complexes of zinc(II) featuring mononuclear **1** and CP structures **3** and **4** (Schemes 1 and 2). The high catalytic activity obtained for all four complexes, particularly for the CP **3** serving as a potential bifunctional (Lewis acid–Lewis base) catalyst, is described in this contribution. Our interest in this system arises in view of the following

considerations: (i) The monoanionic 1,1-dithiocarbamate ligands having identical S[−]S-donor atoms on the same C atom differ remarkably from the monoanionic β -oxodithioester having hard/soft S[−]O-donor atoms on the 1,3-C atoms. The former forms a strained four-membered chelate ring, whereas the latter forms a delocalized stable six-membered chelate ring about the metal center.⁹ Usually the dithiocarbamate ligand is strongly S[−]S-chelating because of the major contribution of resonance form **III** (Scheme S1). A switch to dithiocarbamate complexes may make huge differences in the structures and reactivities of the metal complexes. (ii) The dithiocarbamate unit also offers functionalization of the substituents, which may substantially modify the structures and properties of the complexes. Therefore, it is crucial to make systematic changes in the substituents in order to map out the structures and catalytic activities of the complexes. Compounds containing ferrocene moieties are of considerable interest in the stabilization of interesting structures, electrochemical sensors, and catalysis.^{8j,10} Judiciously, *n*-butyl, *n*-ethylmorpholine, and 2-(diethylamino)ethylamine substituents with different steric and electronic properties were incorporated in the ferrocenyl-derived dithiocarbamate ligands **KL1**–**KL3**, whereas **KL4** was derived from 4-methoxybenzyl and 3-pyridyl substituents (Scheme 1). The presence of additional donor (N and O) atoms on the substituents may facilitate the formation of covalent/noncovalent bonding, thereby organizing the CP and supramolecular architectures. (iii) Zn(II) with a d¹⁰ electronic configuration shows no stereochemical choices arising from the ligand-field stabilization effect. Usually, 4-, 5-, and 6-coordination geometries are stabilized in these complexes. However, the lower coordination numbers can raise up to a maximum of 6-coordination, with the extra bonds provided by the presence of free N-donor atoms on the 2-(diethylamino)-ethylamine sites, thus producing a potentially bifunctional (Lewis acid and Lewis base) catalyst.

■ EXPERIMENTAL SECTION

Materials and Instrumentation. All experiments were performed in the open air at ambient temperature and pressure. The solvents were purified by standard reported procedures and dried before use where necessary.¹¹ The commercially available reagent-grade chemicals ferrocenecarboxaldehyde (98%), 3-picolyamine (99%), 4-(2-aminoethyl)morpholine (99%), and butylamine (99.5%) (all Sigma-Aldrich), 4-methoxybenzaldehyde (98%, Avra), 2-(diethylamino)ethylamine (99%, Alfa-Aesar), and Zn(CH₃CO₂)₂·2H₂O (98.5%, SRL) were used without further purification. The melting points of the complexes were determined in open capillaries using a Gallenkamp apparatus and are uncorrected. Elemental analyses (C, H, and N) and recording of the IR (KBr) spectra are the same as those described elsewhere.^{6i,7e,8j} ¹H and ¹³C{¹H} NMR spectra were recorded in deuterated solvents [CDCl₃, dimethyl sulfoxide (DMSO)-*d*₆, and D₂O] on a JEOL ECZ 500 MHz FT NMR spectrometer. Chemical shifts are quoted in parts per million (ppm) downfield from the internal tetramethylsilane (TMS), and coupling constant (*J*) values are given in hertz (Hz). The UV–vis absorption spectra of the ligands and their zinc(II) complexes were recorded in methanol (MeOH) and dichloromethane solutions, respectively on a Shimadzu UV-1800 instrument. Thin-layer chromatography (TLC) was performed on a Merck 60 F₂₅₄ silica gel, precoated on aluminum plates. Column chromatography was performed on silica gel 100–200 meshes (Merck). The details on single-crystal X-ray data are provided in the crystal discussion section, and powder X-ray diffraction data were collected using a Bruker D8 diffractometer with Cu K α radiation ($\lambda = 1.541836$ Å) in the 2θ range 5–50°, with a scan speed and a step size of 1° and 0.02° min^{−1}, respectively.

Scheme 1. Potassium Salts of the Dithiocarbamate Ligands (KL1–KL4) Used in This Work



Synthesis of Dithiocarbamate Ligands. The potassium salts of the dithiocarbamate ligands KL1–KL4 (Scheme 1) were synthesized by adopting the following procedure, and all ligands are characterized by IR and NMR (^1H and $^{13}\text{C}\{^1\text{H}\}$) and UV–vis spectroscopy.

***N*-Ferrocenylmethyl-*N*-butyl Dithiocarbamate (KL1).** In a typical reaction, ferrocenecarboxaldehyde (0.214 g, 1 mmol) and *n*-butylamine (0.073 g, 1 mmol) were taken in ethanol (EtOH; 15 mL) and refluxed for about 8–10 h at 70 °C. The Schiff base was formed, reduced by using NaBH_4 at 0 °C with an ice bath, and allowed to stir for about 6 h. This yielded a secondary amine, which was extracted using dichloromethane, followed by washing of the dichloromethane layer with water and removal of the solvent. The formed secondary amine was dissolved in 10 mL of tetrahydrofuran (THF), and potassium hydroxide (KOH; 0.056 g, 1 mmol) was added followed by the addition of carbon disulfide (CS_2 ; 0.076 g, 1 mmol) under ice-cold conditions. The reaction mixture was stirred further for 6 h, and the solvent was removed on a rotary evaporator. The product obtained was washed three times with diethyl ether to yield a reddish-brown solid of the *N*-ferrocenylmethyl-*N*-butyl dithiocarbamate (KL1) ligand. Yield: 0.31 g, 82%. ^1H NMR (500 MHz, D_2O): δ 5.15 (s, 2H, $-\text{CH}_2\text{Fc}$), 4.46 (s, 2H, C_5H_4), 4.24 (s, 2H, C_5H_4), 4.29 (s, 5H, C_5H_5), 4.01–3.97 (m, 2H, $-\text{N}-\text{CH}_2-\text{CH}_2-\text{CH}_2-\text{CH}_3$), 1.67–1.64 (m, 2H, $-\text{N}-\text{CH}_2-\text{CH}_2-\text{CH}_2-\text{CH}_3$), 1.33–1.29 (m, 2H, $-\text{N}-\text{CH}_2-\text{CH}_2-\text{CH}_2-\text{CH}_3$), 0.92 (t, $J = 7.3$ Hz, 3H, $-\text{N}-\text{CH}_2-\text{CH}_2-\text{CH}_2-\text{CH}_3$). $^{13}\text{C}\{^1\text{H}\}$ NMR (125 MHz, D_2O): δ 207.5 ($-\text{CS}_2$), 52.9 ($-\text{CH}_2\text{Fc}$), 83.6, 69.6, 69.0, 68.2 ($-\text{Fc}$), 52.6, 28.2, 19.7, 13.4 ($-\text{N}-\text{CH}_2-\text{CH}_2-\text{CH}_2-\text{CH}_3$). IR (KBr, cm^{-1}): 1462 ($\nu_{\text{C}=\text{N}}$), 1025 ($\nu_{\text{C}-\text{S}}$). UV–vis [MeOH; λ_{max} nm (ϵ , $\text{M}^{-1}\text{cm}^{-1}$): 260 (1.3×10^4), 290 (1.1×10^4), 437 (0.07×10^3).

***N*-Ferrocenylmethyl-*N*-ethylmorpholine Dithiocarbamate (KL2).** The potassium salt of ligand KL2 was prepared by the following procedure used in the synthesis of ligand KL1 by utilizing ferrocenecarboxaldehyde (0.214 g, 1 mmol) and 4-(2-aminoethyl)morpholine (0.130 g, 1 mmol). Yield: 0.35 g, 79%. ^1H NMR (500 MHz, $\text{DMSO}-d_6$): δ 5.12 (s, 2H, $-\text{CH}_2\text{Fc}$), 4.40 (s, 2H, C_5H_4), 4.05 (s, 2H, C_5H_4), 4.13 (s, 5H, C_5H_5), 4.00 (t, $J = 5.0$ Hz, 2H, $-\text{N}-\text{CH}_2-\text{CH}_2-\text{N}-(\text{C}_4\text{H}_8)-\text{O}$), 2.50–2.44 (m, 2H, $-\text{N}-\text{CH}_2-\text{CH}_2-\text{N}-(\text{C}_4\text{H}_8)-\text{O}$), 3.54–3.40 (m, 4H, $-\text{N}-\text{CH}_2-\text{CH}_2-\text{N}-(\text{C}_2\text{H}_4-\text{C}_2\text{H}_4)-\text{O}$), 2.44–2.35 (m, 4H, $-\text{N}-\text{CH}_2-\text{CH}_2-\text{N}-(\text{C}_2\text{H}_4-\text{C}_2\text{H}_4)-\text{O}$). $^{13}\text{C}\{^1\text{H}\}$ NMR (125 MHz, $\text{DMSO}-d_6$): δ 213.3 ($-\text{CS}_2$), 54.6 ($-\text{CH}_2\text{Fc}$), 84.9, 69.4, 67.9, 66.8, 65.9, 67.0 ($-\text{Fc}$), 53.4, 53.0, 50.3, 47.3 ($-\text{N}-\text{CH}_2-\text{CH}_2-\text{N}-(\text{C}_4\text{H}_8)-\text{O}$). IR (KBr, cm^{-1}): 1457 ($\nu_{\text{C}=\text{N}}$), 1036 ($\nu_{\text{C}-\text{S}}$). UV–vis [MeOH; λ_{max} nm (ϵ , $\text{M}^{-1}\text{cm}^{-1}$): 260 (1.9×10^4), 290 (1.3×10^4), 437 (0.11×10^3).

***N*-Ferrocenylmethyl-*N*-2-(diethylamino)ethylamine Dithiocarbamate (KL3).** The potassium salt of ligand KL3 was synthesized by adopting the procedure used in the synthesis of ligand KL1 by using ferrocenecarboxaldehyde (0.214 g, 1 mmol) and 2-(diethylamino)ethylamine (0.116 g, 1 mmol). Yield: 0.34 g, 81%. ^1H NMR (500 MHz, $\text{DMSO}-d_6$): δ 5.11 (s, 2H, $-\text{CH}_2\text{Fc}$), 4.38 (s, 2H, C_5H_4), 4.06 (s, 2H, C_5H_4), 4.12 (s, 5H, C_5H_5), 3.93 (t, $J = 5.0$ Hz, 2H, $-\text{N}-\text{CH}_2-\text{CH}_2-\text{N}(\text{CH}_2-\text{CH}_3)_2$), 2.53 (t, $J = 5.0$ Hz, 2H, $-\text{N}-\text{CH}_2-\text{CH}_2-\text{N}(\text{CH}_2-\text{CH}_3)_2$), 2.43 (q, $J = 6.9$ Hz, 4H, $-\text{N}-\text{CH}_2-\text{CH}_2-\text{N}(\text{CH}_2-\text{CH}_3)_2$), 0.94 (t, $J = 7.1$ Hz, 6H, $-\text{N}-\text{CH}_2-\text{CH}_2-\text{N}(\text{CH}_2-\text{CH}_3)_2$). $^{13}\text{C}\{^1\text{H}\}$ NMR (125 MHz, $\text{DMSO}-d_6$): δ 213.0 ($-\text{CS}_2$), 50.7 ($-\text{CH}_2\text{Fc}$), 85.0, 69.3, 68.00, 67.00 ($-\text{Fc}$), 48.6, 46.8, 12.00 ($-\text{N}-\text{CH}_2-\text{CH}_2-\text{N}(\text{CH}_2-\text{CH}_3)_2$). IR (KBr, cm^{-1}): 1449 ($\nu_{\text{C}=\text{N}}$), 1043

($\nu_{\text{C}-\text{S}}$). UV–vis [MeOH; λ_{max} nm (ϵ , $\text{M}^{-1}\text{cm}^{-1}$): 260 (1.6×10^4), 290 (1.0×10^4), 440 (0.05×10^3).

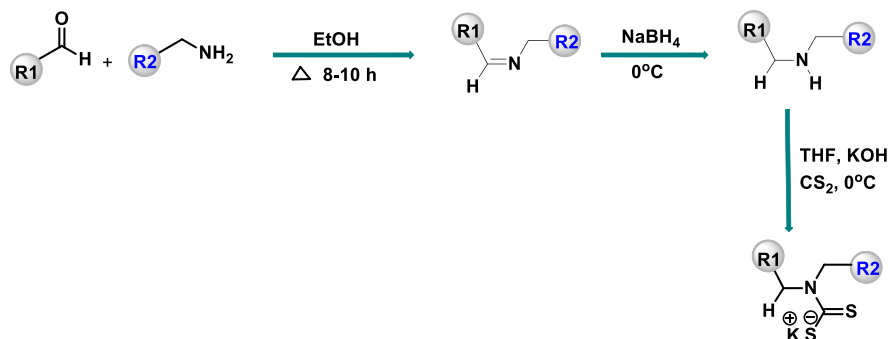
***N*-4-Methoxybenzyl-*N*-3-methylpyridyl Dithiocarbamate (KL4).** The potassium salt of ligand KL4 was prepared by following the procedure used in the synthesis of ligand KL1 by utilizing 4-methoxybenzaldehyde (0.136 g, 1 mmol) and 3-picolyamine (0.108 g, 1 mmol). Yield: 0.30 g, 86%. ^1H NMR (500 MHz, $\text{DMSO}-d_6$): δ 8.45–8.40 (m, 2H, $-\text{C}_6\text{H}_4\text{N}$), 7.70–6.84 (m, 2H, $-\text{C}_6\text{H}_4\text{N}$, 4H, $-\text{C}_6\text{H}_4\text{OCH}_3$), 5.34 (s, 2H, $-\text{CH}_2-\text{C}_6\text{H}_5\text{N}$), 5.28 (s, 2H, $-\text{CH}_2-\text{C}_6\text{H}_4\text{OCH}_3$), 3.72 (s, 3H, $-\text{OCH}_3$). $^{13}\text{C}\{^1\text{H}\}$ NMR (125 MHz, $\text{DMSO}-d_6$): δ 216.5 ($-\text{CS}_2$), 55.1 ($-\text{CH}_2-\text{C}_6\text{H}_4\text{N}$), 53.0 ($-\text{CH}_2-\text{C}_6\text{H}_4\text{OCH}_3$), 51.0 ($-\text{OCH}_3$), 158.1, 148.9, 147.7, 135.2, 134.3, 130.6, 128.9, 123.2, 113.6 ($-\text{C}_6\text{H}_4\text{N}$, $-\text{C}_6\text{H}_4\text{OCH}_3$). IR (KBr, cm^{-1}): 1427 ($\nu_{\text{C}=\text{N}}$), 1040 ($\nu_{\text{C}-\text{S}}$). UV–vis [MeOH; λ_{max} nm (ϵ , $\text{M}^{-1}\text{cm}^{-1}$): 260 (1.5×10^4), 295 (1.1×10^4).

Synthesis and Characterization of Complexes 1–4. The homoleptic zinc(II) dithiocarbamate complexes 1–4 were prepared by adopting the following general procedure.

[Bis(*N*-ferrocenylmethyl-*N*-butyldithiocarbamate-*S* \wedge *S*)zinc(II)] (1). To a stirred 15 mL MeOH solution of the potassium salt of the ligand KL1 (0.385 g, 1 mmol) was slowly added at room temperature 10 mL of a MeOH/water (90:10, v/v) solution of $\text{Zn}(\text{CH}_3\text{COO})_2 \cdot 2\text{H}_2\text{O}$ (0.110 g, 0.5 mmol), and the reaction mixture was further stirred for 2 h. A brown precipitate thus obtained was filtered off, washed with a MeOH/water mixture (3 times), followed by diethyl ether, and dried in air. The auburn needle-shaped single crystals of the complex suitable for X-ray diffraction analysis were obtained from a dichloromethane solution of the compound layered with MeOH within 2 weeks. Empirical formula: $[\text{Zn}(\text{L1})_2]$. Yield: 0.61 g, 81%. Mp: 152–156 °C. ^1H NMR (500 MHz, CDCl_3): δ 4.84 (s, 4H, $-\text{CH}_2\text{Fc}$), 4.40 (s, 4H, C_5H_4), 4.18 (s, 4H, C_5H_4), 4.17 (s, 10H, C_5H_5), 3.70 (t, $J = 5.0$ Hz, 4 H, $-\text{N}-\text{CH}_2-\text{CH}_2-\text{CH}_2-\text{CH}_3$), 1.68–1.29 (m, 8H, $-\text{N}-\text{CH}_2-\text{CH}_2-\text{CH}_2-\text{CH}_3$), 0.92 (t, $J = 7.4$ Hz, 6H, $-\text{N}-\text{CH}_2-\text{CH}_2-\text{CH}_2-\text{CH}_3$). $^{13}\text{C}\{^1\text{H}\}$ NMR (125 MHz, CDCl_3): δ 202.7 ($-\text{CS}_2$), 53.6 ($-\text{CH}_2\text{Fc}$), 81.3, 70.0, 69.0, 68.8 ($-\text{Fc}$), 53.0, 28.7, 20.2, 13.9 ($-\text{N}-\text{CH}_2-\text{CH}_2-\text{CH}_2-\text{CH}_3$). IR (KBr, cm^{-1}): 1498 ($\nu_{\text{C}=\text{N}}$), 1005 ($\nu_{\text{C}-\text{S}}$). Anal. Calcd for $\text{C}_{32}\text{H}_{40}\text{N}_2\text{S}_4\text{Fe}_2\text{Zn}$: C, 50.70; H, 5.32; N, 3.70. Found: C, 50.45; H, 5.30; N, 3.68. UV–vis [CH_2Cl_2 ; λ_{max} nm (ϵ , $\text{M}^{-1}\text{cm}^{-1}$): 265 (1.4×10^4), 450 (0.29×10^3).

[Bis(*N*-ferrocenylmethyl-*N*-ethylmorpholine)dithiocarbamate-*S* \wedge *S*)zinc(II)] (2). Complex 2 was prepared following the procedure used in the synthesis of complex 1 by utilizing ligand KL2 (0.351 g, 1 mmol) and $\text{Zn}(\text{CH}_3\text{COO})_2 \cdot 2\text{H}_2\text{O}$ (0.110 g, 0.5 mmol). Complex 2 was obtained as a brown precipitate. Empirical formula: $[\text{Zn}(\text{L2})_2]$. Yield: 0.68 g, 78%. Mp: 150–155 °C. ^1H NMR (500 MHz, CDCl_3): δ 4.93 (s, 4H, $-\text{CH}_2\text{Fc}$), 4.39 (s, 4H, C_5H_4), 4.19 (s, 4H, C_5H_4), 4.19 (s, 10H, C_5H_5), 3.85 (t, $J = 5.0$ Hz, 4H, $-\text{N}-\text{CH}_2-\text{CH}_2-\text{N}-(\text{C}_4\text{H}_8)-\text{O}$), 2.64 (t, $J = 5.0$ Hz, 4H, $-\text{N}-\text{CH}_2-\text{CH}_2-\text{N}-(\text{C}_4\text{H}_8)-\text{O}$), 3.71–3.69 (m, 8H, $-\text{N}-\text{CH}_2-\text{CH}_2-\text{N}-(\text{C}_2\text{H}_4-\text{C}_2\text{H}_4)-\text{O}$), 2.62–2.48 (m, 8H, $-\text{N}-\text{CH}_2-\text{CH}_2-\text{N}-(\text{C}_2\text{H}_4-\text{C}_2\text{H}_4)-\text{O}$). $^{13}\text{C}\{^1\text{H}\}$ NMR (125 MHz, CDCl_3): δ 203.6 ($-\text{CS}_2$), 55.1 ($-\text{CH}_2\text{Fc}$), 81.2, 70.0, 68.9, 68.8, 67.1 ($-\text{Fc}$), 54.8, 53.9, 49.9 ($-\text{N}-\text{CH}_2-\text{CH}_2-\text{N}-(\text{C}_4\text{H}_8)-\text{O}$). IR (KBr, cm^{-1}): 1486 ($\nu_{\text{C}=\text{N}}$), 1005 ($\nu_{\text{C}-\text{S}}$). Anal. Calcd for $\text{C}_{36}\text{H}_{46}\text{O}_2\text{N}_4\text{S}_4\text{Fe}_2\text{Zn}$: C, 49.58; H, 5.32; N, 6.42. Found: C, 49.15; H, 5.35; N, 6.35. UV–vis [CH_2Cl_2 ; λ_{max} nm (ϵ , $\text{M}^{-1}\text{cm}^{-1}$): 265 (1.4×10^4), 440 (0.22×10^3).

Scheme 2. Synthetic Methodology for the Synthesis of the Potassium Salts of the Dithiocarbamate Ligands KL1–KL4



*Poly[bis{ μ_2 -(*N*-ferrocenylmethyl-*N*-2-(diethylamino)ethylamine- $\kappa^3S^{\wedge}S:N$)}zinc(II)] (3).* Complex 3 was prepared following the procedure used in the synthesis of complex 1 from KL3 (0.428 g, 1 mmol) and $Zn(CH_3COO)_2 \cdot 2H_2O$ (0.110 g, 0.5 mmol). A brown precipitate was obtained in the reaction, and auburn needle-shaped single crystals of 3 suitable for X-ray diffraction analysis were obtained from a dichloromethane solution layered by MeOH within 2–3 weeks. Empirical formula: $[Zn(L3)_2]_n$. Yield: 0.67 g, 80%. Mp: 160 °C. 1H NMR (500 MHz, $CDCl_3$): δ 4.92 (s, 4H, $-CH_2Fc$), 4.41 (s, 4H, C_5H_4), 4.18 (s, 4H, C_5H_4), 4.18 (s, 10H, C_5H_5), 3.79 (t, $J = 5.0$ Hz, 4H, $-N-CH_2-CH_2-N(CH_2-CH_3)_2$), 2.70 (t, $J = 5.0$ Hz, 4H, $-N-CH_2-CH_2-N(CH_2-CH_3)_2$), 2.52 (q, $J = 7.0$ Hz, 8H, $-N-CH_2-CH_2-N(CH_2-CH_3)_2$), 1.02 (t, $J = 7.2$ Hz, 12H, $-N-CH_2-CH_2-N(CH_2-CH_3)_2$). $^{13}C\{^1H\}$ NMR (125 MHz, $CDCl_3$): δ 202.9 ($-CS_2$), 55.1 ($-CH_2Fc$), 81.3, 70.0, 69.0, 68.8 ($-Fc$), 51.6, 49.5, 47.7, 12.3 ($N-CH_2-CH_2-N(CH_2-CH_3)_2$). IR (KBr, cm^{-1}): 1471 ($\nu_{C=N}$), 1020 (ν_{C-S}). Anal. Calcd for $C_{36}H_{50}N_4S_4Fe_2Zn$: C, 51.22; H, 5.97; N, 6.64. Found: C, 51.53; H, 5.99; N, 6.65. UV–vis [CH_2Cl_2 ; λ_{max} nm (ϵ , $M^{-1} cm^{-1}$): 267 (1.3×10^4), 440 (0.26×10^3).

*Poly[bis{ μ_2 -(*N*-4-methoxybenzyl-*N*-3-methylpyridyl)-dithiocarbamate- $\kappa^3S^{\wedge}S:N$)}zinc(II)] (4).* Complex 4 was synthesized following the procedure used in the synthesis of complex 1 from KL4 (0.342 g, 1 mmol) and $Zn(CH_3COO)_2 \cdot 2H_2O$ (0.110 g, 0.5 mmol). A yellow precipitate was obtained in the reaction and light-yellow needle-shaped single crystals of 4 suitable for X-ray diffraction analysis were obtained from a dichloromethane solution layered by MeOH within 2–3 weeks. Empirical formula: $[Zn(L4)_2]$. Yield: 0.57 g, 85%. Mp: 230 °C. 1H NMR (500 MHz, $CDCl_3$): δ 8.93–8.81 (m, 4H, $-C_6H_4N$), 7.76–6.86 (m, 4H, $-C_6H_4N$, 8H, $-C_6H_4OCH_3$), 5.24 (s, 4H, $-CH_2-C_6H_4N$), 5.17 (s, 4H, $-CH_2-C_6H_4OCH_3$), 3.80 (s, 6H, $-OCH_3$). $^{13}C\{^1H\}$ NMR (125 MHz, $CDCl_3$): δ 209.3 ($-CS_2$), 56.8 ($-CH_2-C_6H_4N$), 55.5 ($-CH_2-C_6H_4OCH_3$), 53.6 ($-OCH_3$), 159.6, 148.7, 137.7, 133.1, 129.9, 127.2, 124.5, 114.4 ($-C_6H_4N$, $-C_6H_4OCH_3$). IR (KBr, cm^{-1}): 1455 ($\nu_{C=N}$), 1003 (ν_{C-S}). Anal. Calcd for $C_{30}H_{30}O_2N_4S_4Zn$: C, 53.60; H, 4.50; N, 8.33. Found: C, 53.45; H, 4.56; N, 8.35. UV–vis [CH_2Cl_2 ; λ_{max} nm (ϵ , $M^{-1} cm^{-1}$): 265 (1.2×10^4).

Procedure for the Knoevenagel Condensation Reactions.

Knoevenagel condensation reactions were carried out according to the reported methods.^{5a,12} In a typical reaction, benzaldehyde (0.107 g, 1.0 mmol), malononitrile (0.080 g, 1.2 mmol), and catalyst 3 (0.1 mol %) were added to the reaction flask containing water (2 mL), and the reaction mixture was stirred for 1 h at room temperature. After completion of the reaction (monitored by TLC), the reaction mixture was evaporated to get the crude mass, which was further purified by column chromatography (ethyl acetate/hexane) to yield the pure product. The final product was obtained as a white solid, which was further characterized by NMR spectral analysis. The isolated yield, characterization data, and representative NMR spectra of the Knoevenagel condensation products are given in Data S1 and Figure S12.

Procedure for One-Pot Multicomponent Reactions (Synthesis of 2-Amino-4*H*-chromene Derivatives). In a typical reaction, a reaction flask was charged with a mixture of benzaldehyde

(0.107 g, 1.0 mmol), malononitrile (0.080 g, 1.2 mmol), cyclohexane-1,3-dione (0.112 g, 1.0 mmol), and catalyst 3 (0.1 mol %). EtOH (2 mL) was added to the reaction flask, and the reaction mixture was stirred for 2 h at room temperature. The progress of the reaction was monitored by TLC. The solvent was removed in vacuo to get a crude product, which was purified by column chromatography (ethyl acetate/hexane) to yield the pure product. The isolated yield, characterization data, and representative NMR spectra of 2-amino-4*H*-chromene derivatives are given in Data S2 and Figure S13.

Procedure for the Preparation of Imidazopyrimidine Derivatives. A mixture of benzaldehyde (0.107 g, 1.0 mmol), malononitrile (0.080 g, 1.2 mmol), 2-aminobenzimidazole (0.133, 1.0 mmol), and catalyst 3 (0.1 mol %) was refluxed at 80 °C in EtOH (5 mL). Progress of the reaction was monitored by TLC. Product was obtained as a white solid, which was filtered and washed with EtOH. The obtained solid residue was recrystallized from EtOH to afford the pure product. The isolated yield, characterization data, and representative NMR spectra of 2-amino-4-phenyl-1,4-dihydrobenzo[4,5]imidazopyrimidine-3-carbonitrile derivatives are given in Data S3 and Figure S14.

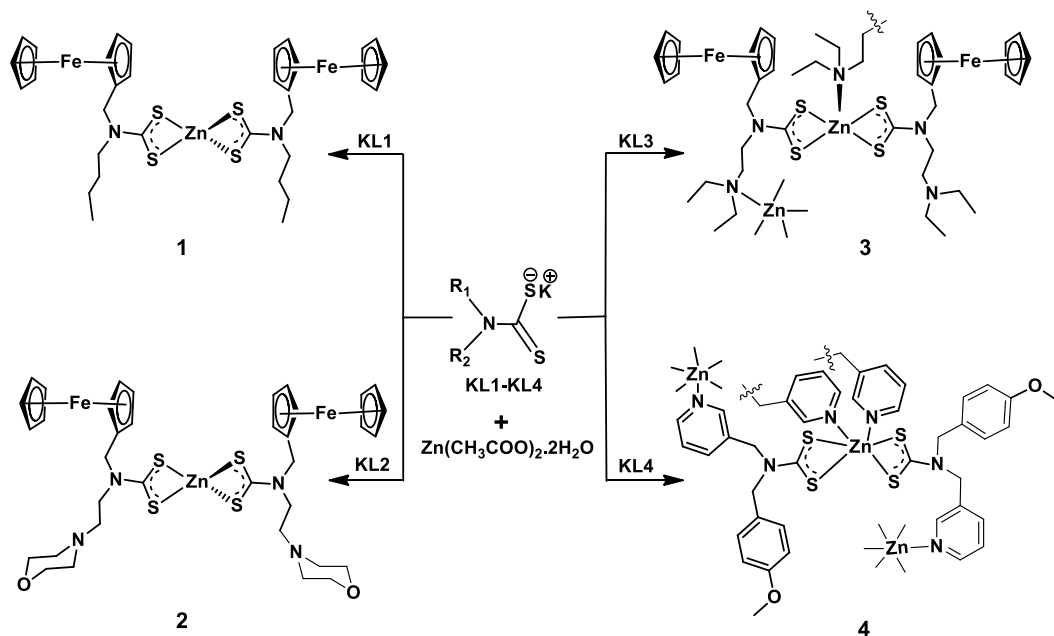
Single-Crystal Structure Determinations. Single-crystal X-ray diffraction data for complex 1 were collected on a Bruker SMART CCD diffractometer with graphite-monochromated Mo $K\alpha$ radiation at 293 K, whereas data for complexes 3 and 4 were collected on an Oxford Diffraction X-calibur CCD diffractometer using Mo $K\alpha$ radiation at 150 K. Data reduction for 1 was carried out using Bruker SAINT,¹³ while those for 3 and 4 were carried out using the CrysAlis program.¹⁴ The structures were solved by direct methods using SHELXS-97¹⁵ and refined on F^2 by a full-matrix least-squares technique using SHELXL2016-6.¹⁶ Non-H atoms were refined anisotropically, and H atoms were geometrically fixed with thermal parameters equivalent to 1.2 times that of the atom to which they were bonded. Diagrams for all complexes were presented using DIAMOND,^{17a} Mercury 3.8,^{17b} and OLEX2^{17c} software. Crystallographic data for 1, 3, and 4 have been deposited at the Cambridge Crystallographic Data Centre as CCDC 2043315, 2043314, and 2043313 respectively.

RESULTS AND DISCUSSION

Synthesis and Spectral Characterization of Ligands and Complexes 1–4. The potassium salts of the dithiocarbamate ligands KL1–KL4 were synthesized by reaction of the appropriate secondary amine and CS_2 in the presence of KOH in a MeOH solvent following the literature procedure (Scheme 2). Secondary amines are prepared from Schiff base condensation of the corresponding aldehyde and primary amine followed by reduction with $NaBH_4$. All ligands were obtained as solid products, which are air- and moisture-stable. These ligands are fully characterized by IR and NMR spectral studies.

The zinc(II) complexes 1–4 with these ligands were synthesized by the treatment of a MeOH solution of

Scheme 3. Synthesis of Complexes 1–4 from the Dithiocarbamate Ligands KL1–KL4 and Metal Salts



$\text{Zn}(\text{CH}_3\text{COO})_2 \cdot 2\text{H}_2\text{O}$ with the ligands KL1–KL4 in a MeOH/water (90:10, v/v) mixture in a 1:2 molar ratio. Complexes were obtained as auburn/light yellow solids in good yield (Scheme 3).

All complexes are air- and moisture-stable solids, which melt in the 150–230 °C temperature range. These complexes are soluble in dichloromethane, *N,N*-dimethylformamide, and DMSO, but they are insoluble in water, EtOH, and MeOH. Complexes are fully characterized by microanalysis and IR and NMR spectral analyses.

IR and NMR Spectral Studies. The IR spectra of all complexes show the $\nu_{\text{C-S}}$ and $\nu_{\text{C-N}}$ vibrations in the 1003–1020 and 1455–1498 cm^{-1} regions, respectively, which are diagnostic of dithiocarbamate ligand coordination.^{8a,b} A significant increase in the $\nu_{\text{C-N}}$ frequency found in complexes compared to the uncoordinated ligands KL1–KL4 (1427–1462 cm^{-1}) may be attributed to π delocalization of the N atom's lone pair of electrons over the NCS_2 backbone (resonance form III in Scheme S1). IR spectra of all ligands and complexes are given in Figures S1 and S2.

The ^1H and $^{13}\text{C}\{^1\text{H}\}$ NMR spectra of complexes 1–4 show resonance signals characteristic of the ligand functionalities. In the ^1H NMR spectra, sharp singlets at chemical shift values of 4.84, 4.93, and 4.92 ppm are present because of the methylene protons attached to the ferrocene fragment in complexes 1–3, respectively. In 4, methylene protons attached to the pyridyl and 4-methoxyphenyl are observed at 5.24 and 5.17 ppm, respectively. The signals for the ferrocene protons are observed at 4.40–4.18 ppm, and the associated aliphatic proton signals are observed at 3.87–0.91 ppm in 1–3. In complex 4, the aromatic proton resonances at 8.93–6.86 ppm and a sharp singlet at 3.80 ppm are assigned to the methoxy protons. In comparison to the free ligands, there is no perceptible shift in the ^1H NMR spectra of the complexes. In the $^{13}\text{C}\{^1\text{H}\}$ NMR spectra, complexes 1–3 show ferrocene carbon signals in the range of 81.3–67.1 ppm; methylene carbon attached to the ferrocene at 53.6, 53.0, and 55.1 ppm, respectively, whereas aliphatic carbon signals are observed in the range of 54.8–12.3 ppm. Complex 4 shows signals at 56.8 and 55.5 ppm for

methylene carbon attached to 3-pyridyl and 4-methoxyphenyl, respectively, aromatic carbon resonances occur at 159.6–114.4 ppm, and the signal at 53.6 ppm is assigned to methoxy carbon. All complexes displayed a single higher-field resonance signal of the NCS_2 group at 202.7–209.3 ppm compared to free ligand signals at 207.5–216.5 ppm, indicating metal–dithiocarbamate ligand coordination due to π delocalization over the NCS_2 backbone.^{8i,j} The ^1H and $^{13}\text{C}\{^1\text{H}\}$ NMR spectra of all ligands and complexes are given in Figures S3 and S4.

Crystal Structures. The solid-state structures for complexes 1, 3, and 4 have been determined by single-crystal X-ray diffraction studies. Single crystals of the complexes suitable for X-ray analysis were obtained by slow evaporation of a solution of the complexes in dichloromethane layered with MeOH. Table 1 summarizes the crystallographic data and structure refinement details, whereas selected bond distances and angles are listed in Table 2.

Complexes 1, 3, and 4 crystallize in the monoclinic system with $P2_1/c$, Cc , and $I2/a$ space groups, respectively. Their molecular structures are illustrated in Figures 1a, 2a, and 4a, respectively. The coordination geometry about the metal center in the mononuclear complex 1 is distorted tetrahedral (Figure 1b) with a ZnS_4 core in which the two symmetric S^\wedgeS -chelating dithiocarbamate ligands L1 are bonded to the metal atom. The Zn–S distances at 2.324(9)–2.348(9) Å are comparable to values found in the literature.^{18a–c} The distortion from ideal tetrahedral geometry indicated with the much smaller bite angles at 78.34(3) and 78.75(3)° and the larger remaining angles in the range 119.77(4)–132.62(4)°. The dihedral angle between the planes formed by the chelate rings Zn(1), S(11), S(13), C(12) and Zn(1), S(41), S(43), C(42) is 79.38(1)°, indicating that the two rings are significantly distorted from the ideal 90°. The two four-membered chelate rings are almost planar showing root-mean-square (rms) deviations of 0.023 and 0.014 Å. The cyclopentadienyl planes of each ferrocene group are nearly parallel, forming angles of 0.6(2) and 1.1(3)°, and the

Table 1. Crystallographic Parameters for Complexes 1, 3, and 4

Compound	1	3	4
chemical formula	C ₃₂ H ₄₀ Fe ₂ N ₂ S ₄ Zn	C ₃₆ H ₅₀ Fe ₂ N ₄ S ₄ Zn	C ₃₀ H ₃₀ N ₄ O ₂ S ₄ Zn
fw (g mol ⁻¹)	757.97	844.11	672.19
cryst syst	monoclinic	monoclinic	monoclinic
space group	P2 ₁ /c	Cc	I2/a
a (Å)	12.4053(12)	19.1088(8)	16.5867(7)
b (Å)	13.7811(13)	13.7251(4)	11.9202(6)
c (Å)	19.8616(19)	14.0935(4)	15.0635(6)
β (deg)	103.240(3)	91.153(3)	96.338(4)
V (Å ³)	3305.3(5)	3695.5(2)	2960.1(2)
Z	4	4	4
T (K)	293(2)	150(2)	150(2)
ρ _{calc} (g cm ⁻³)	1.523	1.517	1.508
μ(Mo Kα) (mm ⁻¹)	1.864	1.677	1.148
F(000)	1568	1760	1392
reflns collected	52215	12041	7492
indep reflns	8222	6405	4137
reflns with I > 2σ(I)	6200	5670	3444
final indices R ₁ ^a , wR ₂ ^b [I > 2σ(I)]	0.0374, 0.0949	0.0413, 0.0843	0.0389, 0.0864
R ₁ ^a , wR ₂ ^b (all data)	0.0636, 0.1198	0.0498, 0.0886	0.0519, 0.0923
GOF ^c	0.975	1.027	1.010
residual electron density, e Å ⁻³	0.481, -0.693	0.479, -0.435	0.521, -0.429

^aR₁ = $\sum |F_o| - |F_c| / \sum |F_o|$. ^bwR₂ = $\{[\sum w(F_o^2 - F_c^2) / \sum w(F_o^2)]\}^{1/2}$. ^cGOF = S = $\{\sum [w(F_o^2 - F_c^2)^2] / (n - p)\}^{1/2}$, where n is the number of reflections and p is the number of the refined parameters.

conformations of the pairs of five-membered rings are nearly eclipsed with torsion angles of 0.8(1) and 7.6(1)°, respectively.

The molecular packing is dominated by close interactions between ferrocene groups. Notable among these is Fe1 with Fe2 on neighboring molecules, thus, Fe1...Fe2 (1 + x, -1 + y, z) at a distance of 7.243(5) Å and Fe1...Fe2 (1 + x, y, z) at a distance of 7.566(5) Å, which gives rise to a zigzag-wave-

layered structure, as shown in Figure 1c. A 1D polymeric chain structure is sustained through C-H...π (ferrocene) interactions (Figure S5), and dimensions are given in Table S1.

Interestingly, the Zn(II) metal center in complex 3 exhibited a distorted square-pyramidal geometry (Figure 2b) around the metal ion in which a Zn(II) ion is bonded with two S^ΔS-chelating dithiocarbamate L3 ligands in the equatorial plane, and a free N53 atom present on the 2-(diethylamino)-ethylamine group of the adjacent molecule is occupying the apical position (Figure 2c). This is also supported by the calculated geometrical index value (τ) 0.258. Thus, a spectacular wavelike 1D CP structure (Figure 2c,d) is formed in which ligand L3 is uniquely bonded in a μ₂,κ³-N,S,S-bridging/chelating fashion. While two of the Zn-S distances in the equatorial plane, i.e., Zn-S13 and Zn-S43 at 2.3841(13) and 2.3589(13) Å, respectively, are similar to those found in complex 1. However, the Zn-S11 and Zn-S41 bond distances of 2.5804(13) and 2.5988(12) Å, respectively, are significantly longer although still within the literature range.^{6i,18} The axial Zn-N53 bond distance is 2.151(4) Å. The two four-membered chelate rings show rms deviations of 0.01 and 0.022 Å, and also they intersect at an angle of 40.3(1)°, thereby showing a tetrahedral twist. The four S atoms in the equatorial plane show a rms deviation of 0.134 Å, and the Zn(II) metal ion is situated 0.537(2) Å away from the plane in the direction of the axial-coordinated N atom of the 2-(diethylamino)-ethylamine group.

Similar to complex 1, complex 3 also displays a wavelike-layered arrangement of the ferrocene moieties along the a crystallographic axis (Figure 3); each Fe atom of a chain is linked to two Fe atoms on the neighboring ferrocene groups at Fe-Fe distances of 7.418(5) and 7.458(5) Å. The distances between two Fe atoms on the adjacent chains are at 6.918(5) and 7.338(6) Å. The cyclopentadienyl planes in each ferrocene moiety are nearly parallel [angles of intersection are 2.57(2)° and 2.83(2)°] and their conformations are nearly eclipsed [1.6 and 1.6° rotations].^{8j} The supramolecular structure is sustained through C-H...π (ZnCS₂, chelate), C-H...π (ferrocene), and H...H interactions (Figures S6-S8), and dimensions are given in Table S1.

Table 2. Bond Lengths (Å) and Bond Angles (deg) in the Metal-Coordinated Sphere of the 1, 3, and 4 Complexes

1		3		4	
Bond Length					
Zn1-S11	2.3307(9)	Zn1-N53 ^a	2.151(4)	Zn1-N34 ^b	2.1768(16)
Zn1-S13	2.3246(8)	Zn1-S11	2.5804(13)	Zn1-S11	2.5896(6)
Zn1-S41	2.3483(8)	Zn1-S13	2.3841(13)	Zn1-S13	2.4807(5)
Zn1-S43	2.3320(9)	Zn1-S41	2.5988(12)		
		Zn1-S43	2.3589(13)		
Bond Angle					
S13-Zn1-S11	78.76(3)	N53 ^a -Zn1-S43	108.99(11)	N34 ^b -Zn1-N34 ^c	86.75(8)
S41-Zn1-S11	119.77(3)	N53 ^a -Zn1-S13	110.55(11)	N34 ^b -Zn1-S13 ^d	101.63(4)
S11-Zn1-S43	131.82(3)	S43-Zn1-S13	140.43(5)	N34 ^c -Zn1-S13 ^d	93.73(4)
S41-Zn1-S43	78.34(3)	S13-Zn1-S11	72.59(4)	S13-Zn1-S13 ^d	158.86(3)
		N53 ^a -Zn1-S41	103.62(10)	N34 ^b -Zn1-S11 ^d	163.30(4)
		S43-Zn1-S41	72.78(4)	N34 ^c -Zn1-S11 ^d	91.29(4)
		S13-Zn1-S41	99.19(4)	S13-Zn1-S11 ^d	95.036(19)
		S11-Zn1-S41	155.93(5)	S13 ^d -Zn1-S11 ^d	70.415(17)
				S11 ^d -Zn1-S11	95.19(3)

^aSymmetry elements: x, 2 - y, 1/2 + z. ^bSymmetry elements: 1 - x, 1 - y, 1 - z. ^cSymmetry elements: 1/2 + x, 3/2 - y, z. ^dSymmetry elements: 3/2 - x, y, 1 - z.

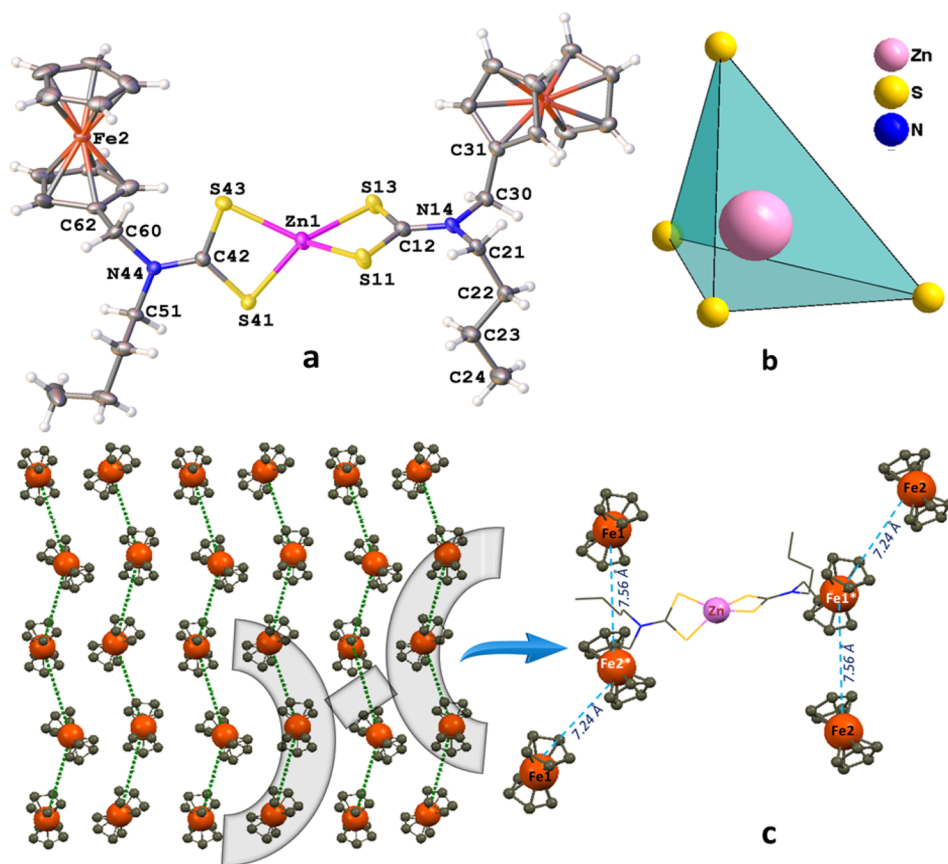


Figure 1. (a) Molecular structure of **1**. Thermal ellipsoids are shown at the 50% probability level. (b) Distorted tetrahedral geometry around the Zn(II) metal ion. (c) Wavelike-layered structure formed by the stacking of ferrocene moieties. The remaining atoms in the molecules are omitted for clarity.

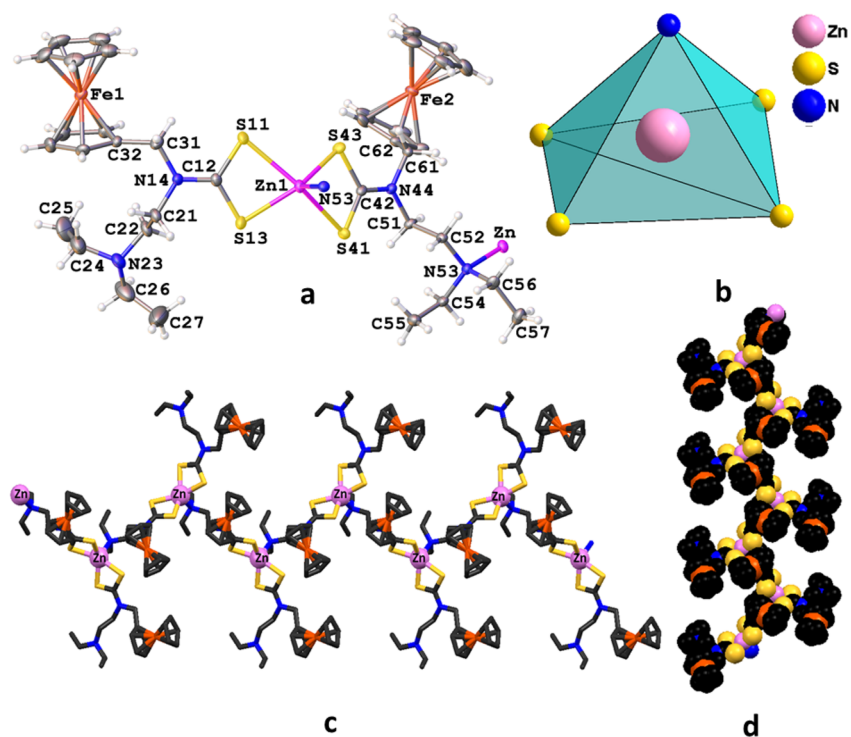


Figure 2. (a) Coordination environment of complex **3** showing the atom-numbering scheme depicted with 50% probability for thermal ellipsoids. (b) Distorted square-pyramidal geometry around the metal atom. (c) 1D CP chain running via Zn–N bonds, resulting in a wavelike structure. (d) View of the packing diagram in the space-filling mode along the *a* axis.

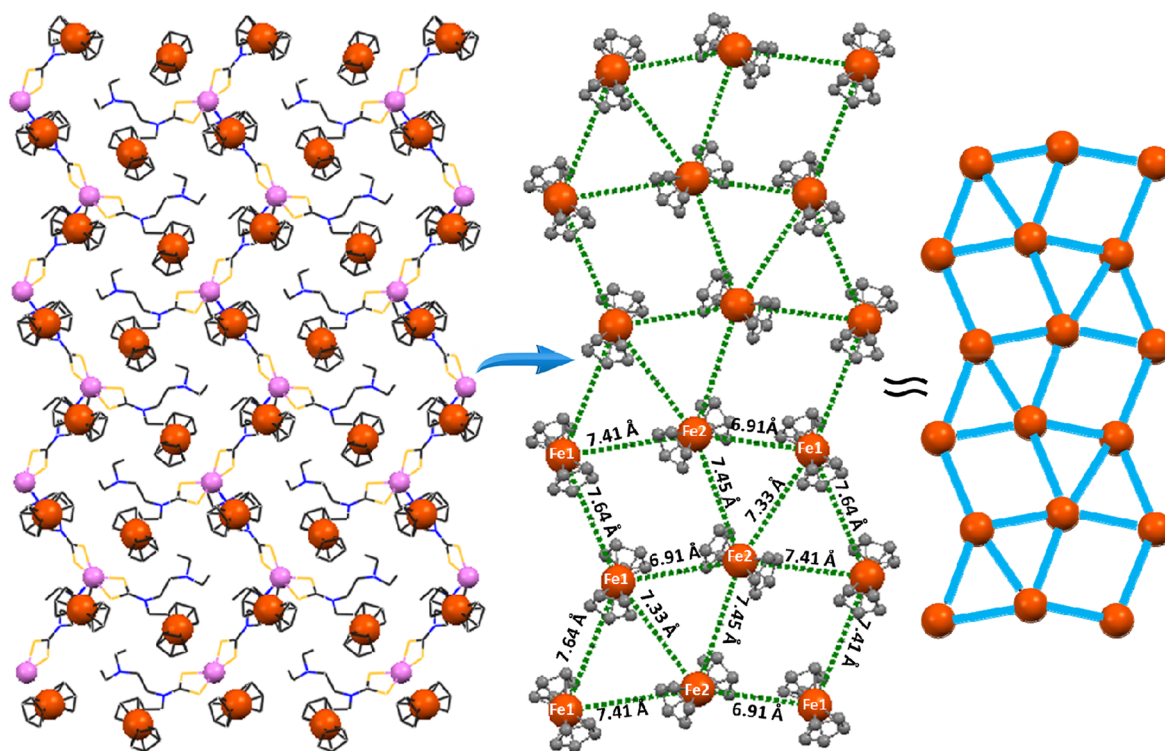


Figure 3. Wavelike architecture formed by the stacking of ferrocene moieties in complex 3 along the crystallographic *a* axis. The molecular skeleton except for the ferrocene moieties is omitted for clarity.

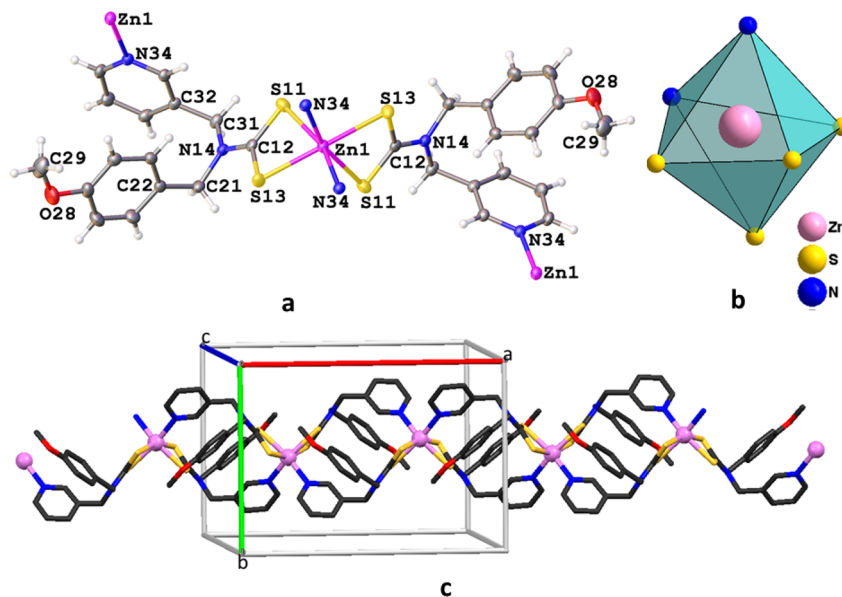


Figure 4. (a) Molecular structure of 4 drawn with 50% probability for thermal ellipsoids. (b) Distorted octahedral geometry around the Zn(II) metal ion. (c) 1D CP chain along the *c* axis in 4 formed through intermolecular Zn–N bonds. H atoms are omitted for the sake of clarity.

Upon switching from complexes 1 and 3 formed with the ferrocenyl-functionalized dithiocarbamate ligands L1–L3 to complex 4 formed with the pyridyl-functionalized dithiocarbamate ligand L4, a different structure is found. The Zn(II) metal ion in complex 4 is situated on a crystallographic 2-fold axis with a distorted 6-coordinate octahedral environment. The metal is bonded to four S atoms from two S,S-chelated dithiocarbamate ligands L4 (Figure 4a,b) in which the Zn–S distances are 2.4807(5) and 2.5896(6) Å.^{18a–c,19} The remaining two mutually cis coordination sites are occupied

by two 3-pyridyl(N) atoms from the two neighboring Zn(L4)₂ units, thus resulting in the formation of an intriguing 1D CP structure (Figure 4c). The Zn–N distances at 2.1768(16) Å are well within the expected range.^{6i,18d} The equatorial plane formed by S11, S13, S13', and N34 show a rms deviation of 0.189 Å, with the metal atom 0.130(1) Å from that plane. However, the N34'–Zn–S11' angle is not linear and subtends an angle of 163.30(4)°, thus considerably deviating from the ideal value of 180°. Complex 4 also forms supramolecular structures similar to those of complexes 1 and 3. These

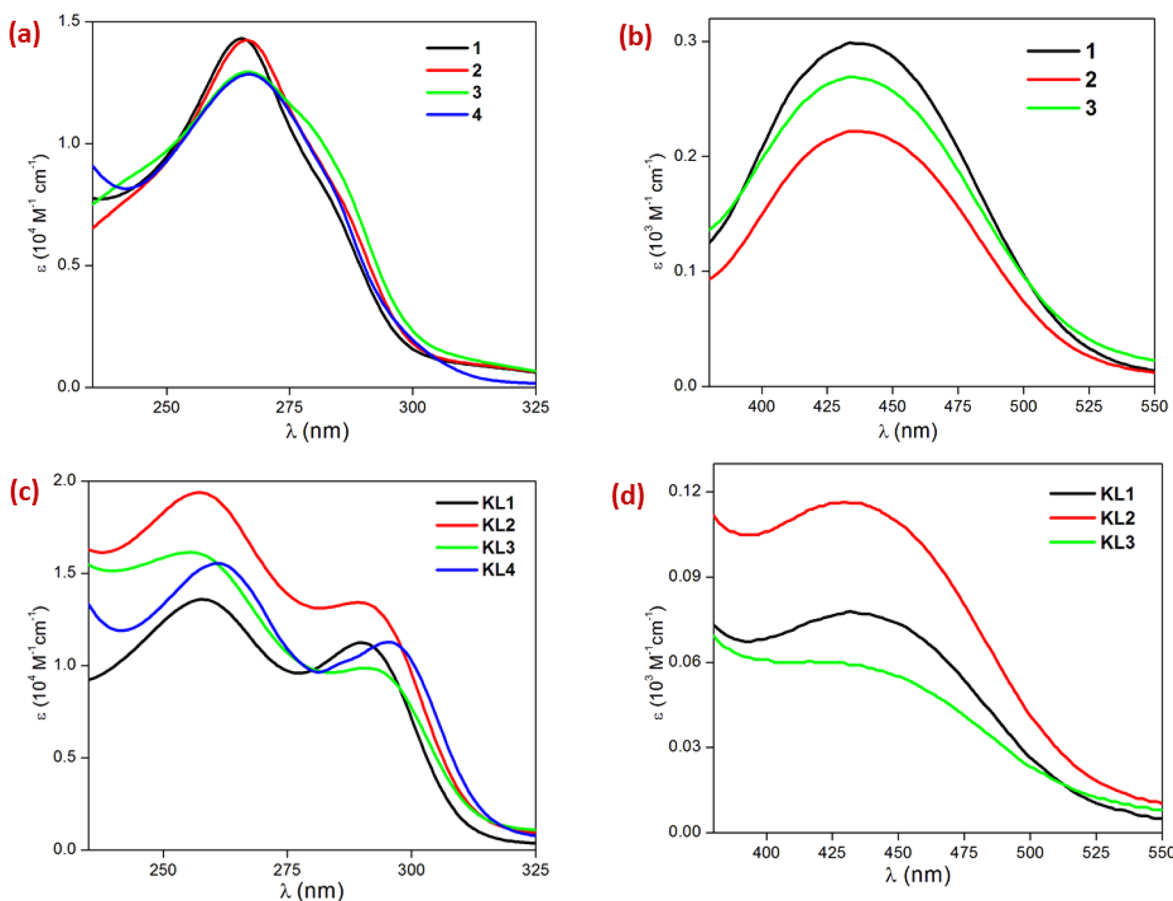


Figure 5. (a) UV-vis absorption spectra of complexes 1–4 in a CH_2Cl_2 solution. (b) d–d absorption band of complexes 1–3. (c) UV-vis absorption spectra of the ligands KL1–KL4 in a MeOH solution. (d) d–d absorption bands of ligands KL1–KL3.

structures are sustained via $\text{C–H}\cdots\pi$ (ZnCS_2 , chelate) and $\text{C–H}\cdots\pi$ (Figures S9 and S10) interactions, and dimensions for these interactions are given in Table S1.

A notable feature in the crystal packing of complexes 3 and 4 is the existence of supramolecular architectures stabilized by $\text{C–H}\cdots\pi$ (ZnCS_2 , chelate) interactions (Figures S6 and S9), thereby strengthening their observed polymeric structures. Tiekink and Zukerman-Schpector have also described the structural features of $\text{C–H}\cdots\pi$ (MCS_2 , chelate) interactions between MS_2C chelate rings in metal bis(1,1-dithiolates); for metal bis(dithio) complexes, the values of $\alpha < 20^\circ$, β ranging from 110 to 180° , and d between 2.4 and 3.6 Å were key to assessing the interactions, where α is the angle between the perpendicular to the ring and the $\text{Cg}\cdots\text{H}$ vector, β the $\text{Cg}\cdots\text{H–C}$ angle, and d the $\text{Cg}\cdots\text{H}$ distance. Recently, we also reported similar $\text{C–H}\cdots\pi$ interactions in heteroleptic nickel(II) 1,1-dithiolatephosphine complexes.^{7e}

In 3, there is an intermolecular ferrocenyl H34 and an intramolecular methylene H56B, which interact with the centroid Cg of ZnS_2C chelate rings, having parameters $\alpha = 19$ and 16° , $\beta = 138$ and 112° , and $d = 2.86$ and 2.96 Å, respectively. In complex 4, ortho H33 of the 3-pyridyl group interacts with Cg having parameters $\alpha = 6^\circ$, $\beta = 113^\circ$, and $d = 2.771$ Å, which are well within the range²⁰ (Figures S6 and S9).

In 1, 3, and 4, the C–N bond lengths of the dithio unit are in the range of 1.315 (4)– 1.336 (3) Å, intermediate between the C–N (1.47 Å) and C=N (1.28 Å) bond lengths, thereby indicating the partial double-bond character of the C–N bond. The C–S bond distances at 1.703 (2)– 1.739 (3) Å are shorter

than the C–S single-bond distance of 1.82 Å due to π delocalization over the NCS_2 backbone. The effect of π delocalization has also been seen in the ^{13}C NMR spectra of the complexes, as discussed in the NMR section.

We also examined the phase purity of the bulk samples of 1, 3, and 4 by comparing the experimental PXRD patterns with the respective simulated powder patterns obtained from the single-crystal data. The experimental and simulated PXRD patterns matched well, indicating the phase purity of the bulk samples (Figure S11).

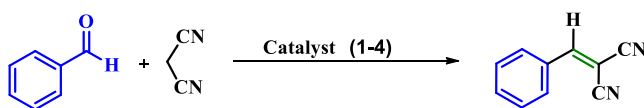
UV-Vis Absorption Spectral Studies. The UV-vis absorption spectra (Figure 5) of the potassium salts of the dithiocarbamate ligands KL1–KL4 in MeOH and their corresponding zinc(II) complexes 1–4 in a dichloromethane solution have been recorded at room temperature at 10^{-4} and 10^{-3} M concentration. The former show medium broad absorptions near 260 nm [$(1.3\text{--}1.9) \times 10^4 \text{ M}^{-1} \text{ cm}^{-1}$] and 290 nm [$(1.0\text{--}1.3) \times 10^4 \text{ M}^{-1} \text{ cm}^{-1}$], whereas the latter show a strong broad band extending between 250 and 300 nm, which are assigned to ligand-centered and metal-perturbed ligand-centered charge-transfer transitions, respectively. In the ligands KL1–KL3 and their respective complexes 1–3, the appearance of an additional medium broad absorption near 450 nm [$(0.22\text{--}0.29) \times 10^3 \text{ M}^{-1} \text{ cm}^{-1}$] is characteristic of the ferrocenyl fragment.^{8j,21}

Catalytic Studies. Complexes 1–4 have been investigated as catalysts for the Knoevenagel condensation and one-pot multicomponent reactions. To the best of our knowledge, this is the first report in which zinc(II) dithiocarbamate ligand

complexes are synthesized and used as catalysts in C–C, C–O, and C–N bond formation reactions. The presence of the exposed Lewis acidic sites [Zn(II) center] and basic sites [2-(diethylamino)ethylamine-N] in the complexes make complexes applicable for organic transformation reactions.

Knoevenagel Condensation Reaction. The catalytic activities of complexes 1–4 were evaluated in the Knoevenagel condensation reaction. The screening of complexes as catalysts was assessed by a model reaction involving the reaction of benzaldehyde (1.0 mmol), malononitrile (1.2 mmol), catalyst (0.5 mol %), and MeOH (2 mL) at 60 °C temperature under air, which resulted in the formation of benzylidene malononitrile as the principal product (Table 3, entries 1–

Table 3. Catalyst Screening for the Knoevenagel Condensation of Benzaldehyde with Malononitrile^a



entry	catalyst	mol %	time	temp (°C)	solvent	yield ^b (%)
1	1	0.5	1 h	60	MeOH	92
2	2	0.5	15 min	60	MeOH	95
3	3	0.5	15 min	60	MeOH	93
4	4	0.5	2 h	60	MeOH	92
5	2	0.5	15 min	25	MeOH	85
6	3	0.5	15 min	25	MeOH	92
7	3	0.1	1 h	25	MeOH	81
8	3	0.2	1 h	25	MeOH	84
9	3	0.3	1 h	25	MeOH	85
10	3	0.1	1 h	25	MeOH	55
11	3	0.1	1 h	25	DCM	94
12	3	0.1	1 h	25	hexane	84
13	3	0.1	1 h	25	DMSO	97
14	3	0.1	1 h	25	THF	77
15	3	0.1	1 h	25	acetonitrile	77
16	3	0.1	1 h	25	toluene	93
17	3	0.1	1 h	25	ethyl acetate	72
18	3	0.1	1 h	25	water	96
19	3	0.1	1 h	25	water	40
20	Zn(OAc) ₂	0.1	1 h	25	water	44
21	KL3	0.1	1 h	25	water	48

^aReaction conditions: benzaldehyde (1.0 mmol) and malononitrile (1.2 mmol) under an air atmosphere. ^bIsolated yield.

4). The catalysis result showed that 100% aldehyde conversion occurred in 1 and 2 h, respectively, when complexes 1 and 4 are used as catalysts, whereas with complexes 2 and 3, this conversion was completed in 15 min with isolated yields of >93%.

The crystal structures of complexes indicated that the metal centers in complexes 1 and 2 displayed tetrahedral geometry, whereas 3 and 4 exhibited square-pyramidal and octahedral geometries, respectively. Therefore, complexes 1–3 have open coordination sites/site at Zn(II) to interact with benzaldehyde, thereby enhancing the electrophilicity of the aldehyde functional group, which resulted in better reactivity. However, high activities of complexes 2 and 3 are attributed to the presence of the free basic moieties morpholine (in 2) and 2-(diethylamino)ethylamine-N (in 3), in addition to an open coordination site. In complex 4, the activation of benzaldehyde

by a metal complex was insignificant because there is no open coordination site at the Zn(II) center and lower activity was expected. The catalytic studies have revealed that complexes 2 and 3 might be behaving as bifunctional catalysts, and therefore high catalytic activities were promoted synergistically by the dual nature (Lewis acidic and basic) of the complexes. To ensure that complex 2 or 3 is the best catalyst, we also performed the same reaction using complexes 2 and 3 at 25 °C and isolated yields were ~85 and 92%, respectively (Table 3, entries 5 and 6). This indicated that the catalytic performance of complex 3 is better than other complexes, which can be explained by considering the presence of a free 2-(diethylamino)ethylamine-N fragment in the 1D-coordinated polymeric structure of the complex (Figure 6).

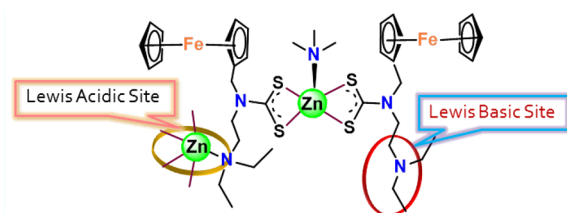
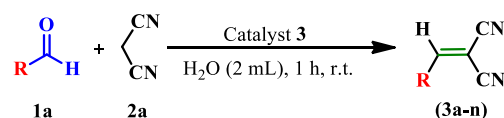


Figure 6. Schematic representation of the bifunctional zinc(II) dithiocarbamate complex 3 with labeled catalytic active sites and a metal coordinating site.

The effect of catalyst loading was also studied. It is revealed that a low catalyst loading resulted in a slight decrease in the catalytic activity (Table 3, entries 7–9). Furthermore, a reaction carried out under neat conditions with 0.1 mol % catalyst 3 at room temperature gave 55% yield in 1 h (Table 3, entry 10). To test the catalytic efficiency in different solvents, experiments were performed in H₂O, DMSO, ethyl acetate, dichloromethane, acetonitrile, hexane, THF, and toluene. It can be revealed from Table 3 (entries 11–18) that higher conversion was achieved in water as a solvent in comparison with other organic solvents under similar reaction conditions and excellent yield (96%) was obtained with 0.1 mol % catalyst 3 and substrates (benzaldehyde and malononitrile) within 1 h of reaction time. The controlled experiments showed that the Knoevenagel condensation reactions also occurred without using a catalyst, which yielded ~40% product in 1 h of reaction time (Table 3, entry 19). Additionally, the reactions utilizing separate Zn(OAc)₂ salt and the dithiocarbamate ligand KL3 result in 44% and 48% isolated products (Table 3, entries 20 and 21), respectively. These controlled experiments clearly indicated that a zinc(II) complex played a crucial role in the Knoevenagel condensation reactions and hence can be efficiently used as a catalyst. The details of comparative studies among various bifunctional MOF/CP catalysts used in the Knoevenagel condensation reactions between benzaldehyde and malononitrile along with our investigation are presented in Table S2. There are several advantages of using our catalyst like performing reaction in water at 25 °C and the isolated yield is >96% in 1 h, which is comparable to the some of the reported catalysts. In addition to this, the low catalyst loading (0.1 mol %) to achieve excellent yields similar to those reported in the literature makes our complex a better catalyst.

Furthermore, the substrate scope for the Knoevenagel condensation reactions catalyzed by complex 3 has been explored, and the results are given in Table 4. The nature of the substituent on the benzaldehyde ring has no significant

Table 4. Knoevenagel Condensation Reactions of Aromatic Aldehydes with Malononitrile Using Catalyst 3^a

Entry	R	Product	Yield ^b %
1	-C ₆ H ₅		96
2	4-FC ₆ H ₄		96
3	4-ClC ₆ H ₄		93
4	4-BrC ₆ H ₄		92
5	4-NO ₂ C ₆ H ₄		95
6	4-CN C ₆ H ₄		96
7	4-OH,3-OMe C ₆ H ₃		95

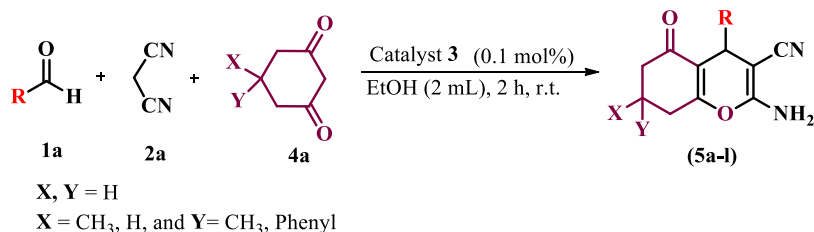
Entry	R	Product	Yield ^b %
8	4-OMeC ₆ H ₄		89
9	4-CH ₃ C ₆ H ₄		91
10	4-CH ₂ CH ₃ C ₆ H ₄		88
11	4-N(Me) ₂ C ₆ H ₄		91
12	1-Naphthalenyl		90
13	3-Pyridyl		84
14	2-Thienyl		82

^aReaction conditions: aldehyde (1.0 mmol), malononitrile (1.2 mmol), water (2 mL), room temperature, and time (1 h) under an air atmosphere.
^bIsolated yield.

effect on the yield of the product, and good-to-excellent yields were obtained with benzaldehyde derivatives containing either electron-withdrawing or -releasing substituents (Table 4, entries 2–11). Similarly, the use of 1-naphthaldehyde (fused aromatic system) also yielded 90% corresponding product (Table 4, entry 12). However, heteroaromatic aldehydes (3-pyridinecarboxaldehyde and 2-thiophenecarboxaldehyde) provided slow reaction and lower yields (Table 4, entries 13 and 14).

Multicomponent Reaction. Synthesis of 2-Amino-4H-chromene Derivatives. The formation of 2-amino-4H-chromene derivatives from the one-pot reaction of aromatic aldehyde, malononitrile, and active methylene cyclic 1,3-diketone has also been explored using complex 3 as a catalyst. The catalytic results are summarized in Table 5. The reaction of benzaldehyde, malononitrile and cyclohexane-1,3-dione in EtOH at room temperature occurring in the absence of catalyst 3 yielded a trace amount of product 5a (Table 5, entry 1).

However, the addition of a catalyst facilitated the reaction and afforded the products 5a–5l with 85–97% isolated yield (Table 5, entries 2–13). The catalyst scope in the chromene derivative synthesis was investigated with aromatic aldehydes (benzaldehyde, 4-nitrobenzaldehyde, 4-methoxybenzaldehyde, and 3-pyridinecarboxaldehyde) and cyclohexane-1,3-diones (cyclohexane-1,3-dione, 5,5-dimethylcyclohexane-1,3-dione, and 5-phenylcyclohexane-1,3-dione). It has been revealed from the catalysis result that with all aromatic aldehydes good-to-excellent yields of the desired product were obtained. The highest yields were obtained with 4-nitrobenzaldehyde irrespective of used 1,3-dione (Table 5, entries 3, 7 and 11). It is interesting to note that when cyclohexane-1,3-dione was replaced with either 5,5-dimethylcyclohexane-1,3-dione (entries 6–9) or 5-phenylcyclohexane-1,3-dione (entries 10–13), excellent yields of the corresponding products were obtained. It can be deduced that complex 3 showed promising catalytic activity for the one-pot multicomponent synthesis of 2-amino-

Table 5. One-Pot Multicomponent Reactions for the Synthesis of 2-Amino-4*H*-chromene Derivatives^a

Entry	R	4a(X, Y)	Product	Yield ^b %
1	-C ₆ H ₅	H, H		- ^c
2	-C ₆ H ₅	H, H		92
3	4-NO ₂ C ₆ H ₄	H, H		95
4	4-OMeC ₆ H ₄	H, H		89
5	3-Pyridyl	H, H		86
6	-C ₆ H ₅	CH ₃ , CH ₃		95
7	4-NO ₂ C ₆ H ₄	CH ₃ , CH ₃		97

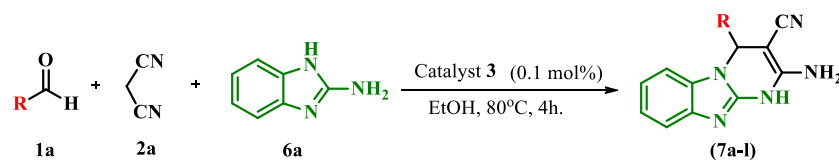
Entry	R	4a(X, Y)	Product	Yield ^b %
8	4-OMeC ₆ H ₄	CH ₃ , CH ₃		85
9	3-Pyridyl	CH ₃ , CH ₃		96
10	-C ₆ H ₅	H, Ph		91
11	4-NO ₂ C ₆ H ₄	H, Ph		96
12	4-OMeC ₆ H ₄	H, Ph		90
13	3-Pyridyl	H, Ph		91

^aReaction conditions: aldehyde (1.0 mmol), malononitrile (1.2 mmol), 1,3-diketone (1.0 mmol), EtOH (2 mL), room temperature, and time (2 h) under an air atmosphere, ^bIsolated yield. ^cReaction without catalyst.

4*H*-chromene derivatives. Kathiresan and co-workers have also achieved a very high yield of 2-amino-4*H*-chromene derivatives (>90%) using Zn-Bp-BTC MOF as a heterogeneous catalyst, but they have run the reaction for longer time (5 h). Similarly, the zinc(II) β-oxodithioester complex also behaves as a bifunctional catalyst for multicomponent reactions, and excellent yields were obtained.⁶¹

Synthesis of Imidazopyrimidine Derivatives. We have also tested the usefulness of complex 3 as a catalyst for the one-pot

synthesis of imidazopyrimidine derivatives. The one-pot reaction of benzaldehyde, malononitrile, and 2-aminobenzimidazole in EtOH was chosen as the model reaction, with 0.1 mol % catalyst 3 resulting in 72% isolated product in 4 h of reaction time at 80 °C refluxed conditions. The results are summarized in Table 6. Similar to the Knoevenagel reaction and one-pot 2-amino-4*H*-chromene synthesis, this reaction also proceeds in the absence of a catalyst, but only a trace amount of the product was obtained (Table 6, entry 1). We

Table 6. One-Pot Multicomponent Reactions for the Synthesis of Imidazopyrimidine Derivatives^a

Entry	R	Product	Yield ^b %	Entry	R	Product	Yield ^b %
1	-C ₆ H ₅		- ^c	8	4-OH, 3-OMe C ₆ H ₃		65
2	-C ₆ H ₅		72	9	4-OMeC ₆ H ₄		68
3	4-FC ₆ H ₄		74	10	4-CH ₃ C ₆ H ₄		70
4	4-ClC ₆ H ₄		75	11	4-CH ₂ CH ₃ C ₆ H ₄		72
5	4-BrC ₆ H ₄		74	12	1-Naphthalenyl		70
6	4-NO ₂ C ₆ H ₄		74	13	3-Pyridyl		71
7	4-CNC ₆ H ₄		78				

^aReaction conditions: aldehyde (1.0 mmol), malononitrile (1.2 mmol), 2-aminobenzimidazole (1.0 mmol), EtOH (5 mL), and 80 °C temperature. ^bIsolated yield (based on the product obtained after crystallization). ^cReaction without catalyst. Time 4 h.

have established the optimized reaction conditions and successfully synthesized a variety of 4-amino-1,2-dihydrobenzo[4,5]imidazo[1,2-a]pyrimidine-3-carbonitrile derivatives **7a–7l** (Table 6, entries 2–13). To further investigate the substrate scope for this reaction, varieties of aromatic aldehydes including substituted benzaldehyde, 1-naphthaldehyde, and 3-pyridinecarboxaldehyde are used in the study. All aldehydes used in this study form the corresponding product in moderate-to-good yield.

To demonstrate the practical synthetic utility of catalyst **3**, a gram-scale experiment was performed for the synthesis of **3a** (Table 4, entry 1). The treatment of benzaldehyde (1.07 g, 10

mmol), malononitrile (0.746 g, 12 mmol), and catalyst **3** (0.1 mol %) in water (20 mL) under the same optimized protocol gave product **3a** in good isolated yield (1.10 g, 72%). Similarly, we have also performed the synthesis of **5a** (Table 5, entry 1) on a gram scale with benzaldehyde (1.07 g, 10 mmol), malononitrile (0.746 g, 12 mmol), cyclohexane-1,3-dione (1.12 g, 10 mmol), and catalyst **3** (0.1 mol %) in EtOH (20 mL), which furnish product **5a** in 77% isolated yield (2.05 g).

Plausible Mechanism for the Knoevenagel and Multicomponent Reactions. The reaction mechanisms for the Knoevenagel condensation and one-pot multicomponent reactions are well established and documented in the

literature.^{5b–d,6h,22,3j,k} The plausible mechanism for organic transformation reactions are depicted in Schemes S2 and S3. As illustrated in Scheme S2, the Knoevenagel condensation reaction of benzaldehyde with malononitrile was initiated with the activation of carbonyl carbon (I) of benzaldehyde by catalyst 3, which increases its electrophilicity. A malononitrile nucleophile, (CN)₂CH[−] (II), is generated by proton abstraction by the basic site (−NEt₂) of the catalyst, which then attacks the activated aldehyde and results in C–C bond formation (III). The next step involves the dissociation of an intermediate from the catalyst surface followed by dehydration to give the benzylidene malononitrile as the Knoevenagel condensation product I, and also a catalyst is regenerated.^{5b,6h}

The plausible mechanistic scheme for both multicomponent reactions is shown in Scheme S3. The multicomponent reaction A involves the attack of enolate generated from 1,3-cyclohexanedione (VI) on the in situ generated Knoevenagel condensation product I, which results in a second C–C bond formation via Michael addition reaction (VII).²² This was followed by tautomerization and intramolecular cyclization (C–O bond formation) to form a 2-amino-4*H*-chromene derivative as the multicomponent reaction product II. Similarly, in the multicomponent reaction B, the in situ generated Knoevenagel condensation product I and 2-amino-benzimidazole led to C–N bond formation via Michael addition reaction (X). Finally, the imidazopyrimidine derivative product III was formed by tautomerization, followed by intramolecular concerted cyclization (second C–N bond formation) of Michael adduct X.^{3j,k}

CONCLUSIONS

New ferrocenyl/pyridyl-functionalized zinc(II) dithiocarbamate complexes 1–4 have been synthesized and fully characterized. Single-crystal X-ray diffraction revealed discrete tetrahedral mononuclear complex 1 and CP structures for 3 and 4. The dithiocarbamate ligands are bonded to the metal center in a S[∧]S bidentate mode in these structures, but additionally in complexes 3 and 4, the N atom on the 2-(diethylamino)ethylamine and 3-pyridyl functionalities on the neighboring molecules are uniquely bonded to the metal center, forming 1D CP structures in which the square-pyramidal and octahedral geometries are established, respectively, about the metal center. Complexes have been applied as catalysts in the Knoevenagel condensation and one-pot multicomponent reactions. In particular, complex 3 serves as an excellent bifunctional heterogeneous catalyst for the Knoevenagel condensation and one-pot multicomponent reactions for the synthesis of useful chemicals. The higher catalytic activity of the 5-coordinate square-pyramidal complex 3 is ascribed to its Lewis acidic character because of the labile coordinative behavior of the metal center. Thus, the steric and electronic properties of the substituents on the dithiocarbamate backbone have a substantial impact on the structures and catalytic properties of the complexes. Notably, the Knoevenagel catalytic transformations of the present series of complexes are superior compared to the β-oxodithioester ligand complexes because of the remarkable differences in the features of the two ligands described (vide supra) in the Introduction. As a result of its mild condition and high efficiency, this catalytic system may be useful in the synthesis of biologically important and other useful chemicals. This study describes an environmentally benign way of carrying out

a zinc-complex-catalyzed C–C/C–O/C–N coupling reaction in water and even in solvent-free conditions.

ASSOCIATED CONTENT

Supporting Information

The Supporting Information is available free of charge at <https://pubs.acs.org/doi/10.1021/acs.inorgchem.1c00162>.

FT-IR and ¹H and ¹³C{¹H} NMR spectra of ligands KL1–KL4 and complexes 1–4, PXRD of complexes, supporting crystallographic figures, characterization data for the Knoevenagel condensation and multicomponent products, and mechanistic schemes for the catalysis reactions (PDF)

Accession Codes

CCDC 2043313–2043315 contain the supplementary crystallographic data for this paper. These data can be obtained free of charge via www.ccdc.cam.ac.uk/data_request/cif, or by emailing data_request@ccdc.cam.ac.uk, or by contacting The Cambridge Crystallographic Data Centre, 12 Union Road, Cambridge CB2 1EZ, UK; fax: +44 1223 336033.

AUTHOR INFORMATION

Corresponding Authors

Kamlesh Kumar – Department of Chemistry, Institute of Science, Banaras Hindu University, Varanasi 221005, India; Email: kamlesh.kumar@bhu.ac.in

Nanhai Singh – Department of Chemistry, Institute of Science, Banaras Hindu University, Varanasi 221005, India;  orcid.org/0000-0003-1578-5456; Email: nsinghbhu@gmail.com, nsingh@bhu.ac.in

Authors

Anamika – Department of Chemistry, Institute of Science, Banaras Hindu University, Varanasi 221005, India

Chote Lal Yadav – Department of Chemistry, Institute of Science, Banaras Hindu University, Varanasi 221005, India

Michael G. B. Drew – Department of Chemistry, University of Reading, Whiteknights, Reading RG6 6AD, U.K.

Complete contact information is available at: <https://pubs.acs.org/doi/10.1021/acs.inorgchem.1c00162>

Author Contributions

The manuscript was written through contributions of all authors.

Notes

The authors declare no competing financial interest.

ACKNOWLEDGMENTS

Financial support from the UGC-BSR Faculty Fellow [Grant F.18-1/2011(BSR)] to N.S., a UGC-BSR Research Start-Up Grant [Grant F.30-431/2018(BSR)] and a Banaras Hindu University-Seed Grant under IoE scheme to K.K., a CSIR-SRF fellowship to Anamika, and the Department of Chemistry, Institute of Science, Banaras Hindu University, UGC CAS-II, for infrastructural facilities is gratefully acknowledged. M.G.B.D. thanks the University of Reading and EPSRC (U.K.) for funds for the diffractometer used for the data collection of structures 3 and 4.

REFERENCES

(1) Freeman, F. Properties and reactions of ylidenemalononitriles. *Chem. Rev.* 1980, 80, 329–350.

(2) (a) Thomas, N.; Zachariah, S. M. Pharmacological activities of chromene derivatives: An overview. *Asian J. Pharm. Clin. Res.* **2013**, *6*, 11–15. (b) Pratap, R.; Ram, V. J. Natural and Synthetic Chromenes, Fused Chromenes, and Versatility of Dihydrobenzo[h]chromenes in Organic Synthesis. *Chem. Rev.* **2014**, *114*, 10476–10526. (c) Yu, D.; Chen, C. H.; Bossi, A.; Lee, K. H. Anti-AIDS agents. Substituted 3'R,4'R-di-O-(–)-camphanoyl-2',2'dimethyldihydropyrano[2,3-f]-chromene (DCP) analogues as potent anti-HIV agents. *J. Med. Chem.* **2004**, *47*, 4072–4082. (d) Zhou, T.; Shi, Q.; Chen, C. H.; Zhu, H.; Huang, L.; Ho, P.; Lee, K. H. Anti-AIDS agents 79. Design, synthesis, molecular modeling, and structure-activity relationships of novel dicamphanoyl-20, 20-dimethyldihydropyranochromone (DCP) analogs as potent anti-HIV agents. *Bioorg. Med. Chem.* **2010**, *18*, 6678–6689. (e) Raj, T.; Bhatia, R. K.; Kapur, A.; Sharma, M.; Saxena, A. K.; Ishar, M. P. S. Cytotoxic activity of 3-(5-phenyl-3H-[1,2,4] dithiazolo-3-yl) chromen-4-ones and 4-oxo-4H-chromene-3-carbothioic acid N-phenylamides. *Eur. J. Med. Chem.* **2010**, *45*, 790–794. (f) Martínez-Grau, A.; Marco, J. Friedländer reaction on 2-amino-3-cyano-4H-pyrans: synthesis of derivatives of 4H-pyran [2, 3-b] quinoline, new tacrine analogues. *J. Bioorg. Med. Chem. Lett.* **1997**, *7*, 3165–3170.

(3) (a) Chitra, S.; Devanathan, D.; Pandiarajan, K. Synthesis and in vitro microbiological evaluation of novel 4-aryl-5-isopropoxycarbonyl-6-methyl-3, 4-dihydropyrimidinones. *Eur. J. Med. Chem.* **2010**, *45*, 367–371. (b) Deshmukh, M. B.; Salunkhe, S. M.; Patil, D. R.; Anbhule, P. V. A novel and efficient one step synthesis of 2-amino-5-cyano-6-hydroxy-4-aryl pyrimidines and their anti-bacterial activity. *Eur. J. Med. Chem.* **2009**, *44*, 2651–2654. (c) Mokale, S. N.; Shinde, S. S.; Elgire, R. D.; Sangshetti, J. N.; Shinde, D. B. Synthesis and anti-inflammatory activity of some 3-(4,6-disubstituted-2-thioxo-1, 2, 3, 4-tetrahydropyrimidin-5-yl) propanoic acid derivatives. *Bioorg. Med. Chem. Lett.* **2010**, *20*, 4424–4426. (d) Trivedi, A. R.; Bhuvu, V. R.; Dholaria, B. H.; Dodiya, D. K.; Kataria, V. B.; Shah, V. H. Novel dihydropyrimidines as a potential new class of antitubercular agents. *Bioorg. Med. Chem. Lett.* **2010**, *20*, 6100–6102. (e) Prashantha Kumar, B.; Sankar, G.; Nasir Baig, R. B.; Chandrashekar, S. Novel Biginelli dihydropyrimidines with potential anticancer activity: a parallel synthesis and CoMSIA study. *Eur. J. Med. Chem.* **2009**, *44*, 4192–4198. (f) Chiang, A. N.; Valderramos, J. C.; Balachandran, R.; Chovatya, R. J.; Mead, B. P.; Schneider, C.; Bell, S. L.; Klein, M. G.; Huryn, D. M.; Chen, X. S.; Day, B. W.; Fidock, D. A.; Wipf, P.; Brodsky, J. L. Select pyrimidinones inhibit the propagation of the malarial parasite, *Plasmodium falciparum*. *Bioorg. Med. Chem.* **2009**, *17*, 1527–1533. (g) Alam, O.; Khan, S. A.; Siddiqui, N.; Ahsan, W.; Verma, S. P.; Gilani, S. J. Antihypertensive activity of newer 1,4-dihydro-5-pyrimidine carboxamides: Synthesis and pharmacological evaluation. *Eur. J. Med. Chem.* **2010**, *45*, 5113–5119. (h) Badawey, E. S. A. M.; Kappe, T. Benzimidazole condensed ring system. IX. Potential antineoplastics. New synthesis of some pyrido[1,2-a]-benzimidazoles and related derivative. *Eur. J. Med. Chem.* **1995**, *30*, 327–332. (i) Alajarin, R.; Vaquero, J. J.; Alvarez-Builla, J.; de Casa-Juana, M. F.; Sunkel, C.; Priego, J. G.; Gomez-Sal, P.; Torres, R. Imidazo[1,2-a]pyrimidine and benzo[4,5] Imidazo- [1,2-a]pyrimidine derivatives as calcium antagonists. *Bioorg. Med. Chem.* **1994**, *2*, 323–329. (j) Hemmati, B.; Javanshir, S.; Dolatkah, Z. Hybrid magnetic Irish moss/Fe₃O₄ as a nano-biocatalyst for synthesis of imidazopyrimidine derivatives. *RSC Adv.* **2016**, *6*, 50431–50436. (k) Verma, P.; Pal, S.; Chauhan, S.; Mishra, A.; Sinha, I.; Singh, S.; Srivastava, V. Starch functionalized magnetite nanoparticles: A green, biocatalyst for one-pot multicomponent synthesis of imidazopyrimidine derivatives in aqueous medium under ultrasound irradiation. *J. Mol. Struct.* **2020**, *1203*, 127410.

(4) (a) Protopopov, M. V.; Ostrynska, O. V.; Starosyla, S. A.; Vodolazhenko, M. A.; Sirko, S. M.; Gorobets, N. Y.; Bdzholva, V.; Desenko, S. M.; Yarmoluk, S. M. Dihydrobenzo [4, 5] imidazo [1, 2-a] pyrimidine-4-ones as a new class of CK2 inhibitors. *Mol. Diversity* **2018**, *22*, 991–998. (b) Goodacre, S. C.; Street, L. J.; Hallett, D. J.; Crawforth, J. M.; Kelly, S.; Owens, A. P.; Blackaby, W. P.; Lewis, R. T.; Stanley, J.; Smith, A. J.; Ferris, P.; Sohal, B.; Cook, S. M.; Pike, A.; Brown, N.; Wafford, K. A.; Marshall, G.; Castro, J. L.; Atack, J. R.

Imidazo [1, 2-a] pyrimidines as functionally selective and orally bioavailable GABAA α 2/ α 3 binding site agonists for the treatment of anxiety disorders. *J. Med. Chem.* **2006**, *49*, 35–38. (c) Kaur, N.; Kaur, K.; Raj, T.; Kaur, G.; Singh, A.; Aree, T.; Park, S. J.; Kim, T. J.; Singh, N.; Jang, D. O. One-pot synthesis of tricyclic dihydropyrimidine derivatives and their biological evaluation. *Tetrahedron* **2015**, *71*, 332–337.

(5) (a) Tran, U. P.; Le, K. K.; Phan, N. T. Expanding applications of metal–organic frameworks: zeolite imidazolate framework ZIF-8 as an efficient heterogeneous catalyst for the Knoevenagel reaction. *ACS Catal.* **2011**, *1*, 120–127. (b) Parmar, B.; Patel, P.; Murali, V.; Rachuri, Y.; Kureshy, R. I.; Khan, N. H.; Suresh, E. Efficient heterogeneous catalysis by dual ligand Zn (II)/Cd (II) MOFs for the Knoevenagel condensation reaction: adaptable synthetic routes, characterization, crystal structures and luminescence studies. *Inorg. Chem. Front.* **2018**, *5*, 2630–2640. (c) Varadwaj, G. B. B.; Rana, S.; Parida, K. M. Amine functionalized K10 montmorillonite: a solid acid–base catalyst for the Knoevenagel condensation reaction. *Dalton Trans.* **2013**, *42*, 5122–5129. (d) Gándara, F.; Medina, M. E.; Snejko, N.; Gómez-Lor, B.; Iglesias, M.; Gutiérrez-Puebla, E.; Monge, M. A. Two-Dimensional Hybrid Germanium Zeotype Formed by Selective Coordination of the trans-1, 2-Diaminocyclohexane Isomer to the Ge Atom: Heterogeneous Acid–Base Bifunctional Catalyst. *Inorg. Chem.* **2008**, *47*, 6791–6795. (e) Neogi, S.; Sharma, M. K.; Bharadwaj, P. K. Knoevenagel condensation and cyanosilylation reactions catalyzed by a MOF containing coordinatively unsaturated Zn (II) centers. *J. Mol. Catal. A: Chem.* **2009**, *299*, 1–4. (f) Gascon, J.; Aktay, U.; Hernandez-Alonso, M. D.; van Klink, G. P.; Kapteijn, F. Amino-based metal-organic frameworks as stable, highly active basic catalysts. *J. Catal.* **2009**, *261*, 75–87. (g) Parida, K. M.; Rath, D. Amine functionalized MCM-41: An active and reusable catalyst for Knoevenagel condensation reaction. *J. Mol. Catal. A: Chem.* **2009**, *310*, 93–100. (h) Martins, L.; Hölderich, W.; Hammer, P.; Cardoso, D. Preparation of different basic Si–MCM-41 catalysts and application in the Knoevenagel and Claisen–Schmidt condensation reactions. *J. Catal.* **2010**, *271*, 220–227. (i) He, Z.; Zhao, X.; Pan, X.; Li, Y.; Wang, X.; Xu, H.; Xu, Z. Ligand geometry controlling Zn-MOF partial structures for their catalytic performance in Knoevenagel condensation. *RSC Adv.* **2019**, *9*, 25170–25176. (j) Wang, J.; Han, Y.; Xu, H.; Xu, Z. L. Microporous assembly and shape control of a new Zn metal–organic framework: Morphology-dependent catalytic performance. *Appl. Organomet. Chem.* **2018**, *32*, e4097. (k) Li, Y.; Su, Y.; Xu, J.; Xu, Z. L.; Xu, H. Shape-Controlled Micro-Crystals of Chain-Like Zn (II) Coordination Polymer [Zn (NIA) EDA] α and Its Catalytic Performance. *Bull. Chem. Soc. Jpn.* **2017**, *90*, 1152–1156.

(6) (a) Park, J.; Li, J.-R.; Chen, Y.-P.; Yu, J.; Yakovenko, A. A.; Wang, Z. U.; Sun, L.-B.; Balbuena, P. B.; Zhou, H.-C. A versatile metal–organic framework for carbon dioxide capture and cooperative catalysis. *Chem. Commun.* **2012**, *48*, 9995–9997. (b) Miao, Z.; Luan, Y.; Qi, C.; Ramella, D. The synthesis of a bifunctional copper metal organic framework and its application in the aerobic oxidation/Knoevenagel condensation sequential reaction. *Dalton Trans.* **2016**, *45*, 13917–13924. (c) Gao, M. L.; Qi, M. H.; Liu, L.; Han, Z. B. An exceptionally stable core–shell MOF/COF bifunctional catalyst for a highly efficient cascade deacetalization–Knoevenagel condensation reaction. *Chem. Commun.* **2019**, *55*, 6377–6380. (d) Qi, M. H.; Gao, M. L.; Liu, L.; Han, Z. B. Robust Bifunctional Core–Shell MOF@POP Catalyst for One-Pot Tandem Reaction. *Inorg. Chem.* **2018**, *57*, 14467–14470. (e) Srirambalaji, R.; Hong, S.; Natarajan, R.; Yoon, M.; Hota, R.; Kim, Y.; Ho Ko, Y.; Kim, K. Tandem catalysis with a bifunctional site-isolated Lewis acid–Bronsted base metal–organic framework, NH₂-MIL-101 (Al). *Chem. Commun.* **2012**, *48*, 11650–11652. (f) Yang, Y.; Yao, H.-F.; Xi, F.-G.; Gao, E.-Q. Amino-functionalized Zr(IV) metal–organic framework as bifunctional acid–base catalyst for Knoevenagel condensation. *J. Mol. Catal. A: Chem.* **2014**, *390*, 198–205. (g) Yao, C.; Zhou, S.; Kang, X.; Zhao, Y.; Yan, R.; Zhang, Y.; Wen, L. A Cationic Zinc-Organic Framework with Lewis Acidic and Basic Bifunctional Sites as an Efficient Solvent-Free Catalyst: CO₂ Fixation and Knoevenagel Condensation Reaction.

- Inorg. Chem.* **2018**, *57*, 11157–11164. (h) Madasamy, K.; Kumaraguru, S.; Sankar, V.; Mannathan, S.; Kathiresan, M. Zn based Metal Organic Frameworks as a Heterogeneous Catalyst for C–C Bond Formation Reactions. *New J. Chem.* **2019**, *43*, 3793–3800. (i) Yadav, C. L.; Anamika; Rajput, G.; Kumar, K.; Drew, M. G.; Singh, N. Effect of Substituents on the Crystal Structures, Optical Properties, and Catalytic Activity of Homoleptic Zn (II) and Cd (II) β -oxodithioester Complexes. *Inorg. Chem.* **2020**, *59*, 11417–11431. (j) Shiju, N. R.; Alberts, A. H.; Khalid, S.; Brown, D. R.; Rothenberg, G. Mesoporous silica with site-isolated amine and phosphotungstic acid groups: a solid catalyst with tunable antagonistic functions for one-pot tandem reactions. *Angew. Chem., Int. Ed.* **2011**, *50*, 9615–9619.
- (7) (a) Evans, D. A.; Michael, F. E.; Tedrow, J. S.; Campos, K. R. Application of chiral mixed phosphorus/sulfur ligands to enantioselective rhodium-catalyzed dehydroamino acid hydrogenation and ketone hydrosilylation processes. *J. Am. Chem. Soc.* **2003**, *125*, 3534–3543. (b) Mancheño, O. G.; Arrayás, R. G.; Carretero, J. C. Palladium Complexes of Chiral Planar 1-Phosphino-2-sulfonylferrocenes as Efficient Catalysts in Enantioselective Diels–Alder Reactions. *Organometallics* **2005**, *24*, 557–561. (c) Xia, Q. H.; Ge, H. Q.; Ye, C. P.; Liu, Z. M.; Su, K. X. Advances in homogeneous and heterogeneous catalytic asymmetric epoxidation. *Chem. Rev.* **2005**, *105*, 1603–1662. (d) Hogarth, G.; Pateman, A.; Sella, A. Multiple nitrene insertions into the copper–sulfur bonds of dithiocarbamate ligands: synthesis and molecular structure of the tetraamido complex $[\text{Cu}\{\eta^2\text{-RN}(\text{NMe}_2)\text{SNR}\}_2]$ (R = $\text{SO}_2\text{C}_6\text{H}_4\text{Me-p}$). *Chem. Commun.* **1997**, 1029–1030. (e) Anamika; Yadav, D. K.; Manar, K. K.; Yadav, C. L.; Kumar, K.; Ganesan, V.; Drew, M. G. B.; Singh, N. New heteroleptic $[\text{Ni}(\text{II}) \text{1,1-dithiolate-phosphine}]$ complexes: synthesis, characterization and electrocatalytic oxygen evolution studies. *Dalton Trans.* **2020**, 49, 3592–3605. (f) Anamika; Agrahari, A. K.; Manar, K. K.; Yadav, C. L.; Tiwari, V. K.; Drew, M. G. B.; Singh, N. Highly efficient structurally characterised novel precatalysts: di- and mononuclear heteroleptic Cu(I) dioxanthate/xanthate–phosphine complexes for azide–alkyne cycloadditions. *New J. Chem.* **2019**, *43*, 8939–8949. (g) Singh, A. K.; Yadav, C. L.; Mishra, K. B.; Singh, S. K.; Gupta, A. N.; Tiwari, V. K.; Drew, M. G.; Singh, N. Highly efficient and recyclable pre-catalysts based on mono- and dinuclear heteroleptic Cu(I) dithio-PPh₃ complexes to produce variety of glycoconjugate triazoles. *Mol. Catal.* **2019**, *470*, 152–163. (h) Kumari, K.; Singh, A. S.; Manar, K. K.; Yadav, C. L.; Tiwari, V. K.; Drew, M. G.; Singh, N. Catalytic activity of new heteroleptic $[\text{Cu}(\text{PPh}_3)_2(\beta\text{-oxodithioester})]$ complexes: click derived triazolyl glycoconjugates. *New J. Chem.* **2019**, *43*, 1166–1176. (i) Kumari, K.; Kumar, S.; Singh, K. N.; Drew, M. G.; Singh, N. Synthesis and characterization of new square planar heteroleptic cationic complexes $[\text{Ni}(\text{II}) \beta\text{-oxodithioester-dppe}]^+$; their use as a catalyst for Chan–Lam coupling. *New J. Chem.* **2020**, *44*, 12143–12153.
- (8) (a) Coucouvanis, D. The Chemistry of the dithioacid and 1,1-dithiolate complexes. *Prog. Inorg. Chem.* **2007**, *26*, 301–469. (b) Hogarth, G. Transition metal dithiocarbamates. *Prog. Inorg. Chem.* **2005**, *53*, 71–561. (c) Hogarth, G. Metal-dithiocarbamate complexes: chemistry and biological activity. *Mini-Rev. Med. Chem.* **2012**, *12*, 1202–1215. (d) Mensforth, E. J.; Hill, M. R.; Batten, S. R. Coordination polymers of sulphur-donor ligands. *Inorg. Chim. Acta* **2013**, *403*, 9–24. (e) Nieuwenhuizen, P. J.; Reedijk, J.; Van Duin, M.; McGill, W. J. Thiuram- and dithiocarbamate-accelerated sulfur vulcanization from the chemist's perspective; methods, materials and mechanisms reviewed. *Rubber Chem. Technol.* **1997**, *70*, 368–429. (f) Ramasamy, K.; Kuznetsov, V. L.; Gopal, K.; Malik, M. A.; Raftery, J.; Edwards, P. P.; O'Brien, P. Organotin dithiocarbamates: single-source precursors for tin sulfide thin films by aerosol-assisted chemical vapor deposition (AACVD). *Chemistry of Materials. Chem. Mater.* **2013**, *25*, 266–276. (g) Gu, F.; Li, C.; Wang, S. Solution–chemical synthesis of carbon nanotube/ZnS nanoparticle core/shell heterostructures. *Inorg. Chem.* **2007**, *46*, 5343–5348. (h) Kumar, A.; Chauhan, R.; Molloy, K. C.; Kociok-Köhn, G.; Bahadur, L.; Singh, N. Synthesis, Structure and Light-Harvesting Properties of Some New Transition-Metal Dithiocarbamates Involving Ferrocene. *Chem. - Eur. J.* **2010**, *16*, 4307–4314. (i) Singh, V.; Chauhan, R.; Gupta, A. N.; Kumar, V.; Drew, M. G. B.; Bahadur, L.; Singh, N. Photosensitizing activity of ferrocenyl bearing Ni (II) and Cu(II) dithiocarbamates in dye sensitized TiO₂ solar cells. *Dalton Trans.* **2014**, 43, 4752–4761. (j) Manar, K. K.; Yadav, C. L.; Tiwari, N.; Singh, K. R.; Kumar, A.; Drew, M. G.; Singh, N. Effect of functionalities on the crystal structures of new zinc(II) dithiocarbamates: a combined anti-leishmanial and thermal decomposition study. *CrystEngComm* **2017**, *19*, 2660–2672.
- (9) (a) García-Orozco, I.; Ortega-Alfaro, M. C.; López-Cortés, J. G.; Toscano, R. A.; Alvarez-Toledano, C. Synthesis and Characterization of Novel Dinuclear Copper(I) Complexes. Dimerization of $[\text{CuL}(\text{PPh}_3)_2](\text{L} = \text{methyl 3-hydroxy-3-(p-R-phenyl)-2-propenedithioate})$. *Inorg. Chem.* **2006**, *45*, 1766–1773. (b) Rajput, G.; Yadav, M. K.; Drew, M. G.; Singh, N. Influence of the ligand frameworks on the coordination environment and properties of new phenylmercury (ii) β -oxodithioester complexes. *Dalton Trans.* **2015**, 44, 5909–5916. (c) Yadav, C. L.; Rajput, G.; Manar, K. K.; Kumari, K.; Drew, M. G.; Singh, N. Cooperative metal–ligand influence on the formation of coordination polymers, and conducting and photophysical properties of Tl(I) complexes. *Dalton Trans.* **2018**, 47, 16264–16278.
- (10) (a) Sadhukhan, N.; Bera, J. K. Mixed-Metal Assemblies Involving Ferrocene–Naphthyridine Hybrids. *Inorg. Chem.* **2009**, *48*, 978–990. (b) Togni, A.; Hayashi, T. Ferrocenes: Homogeneous Catalysis. *Organic Synthesis. Material Synthesis*; Wiley, 1995.
- (11) Furniss, B. S.; Hannaford, A. J.; Smith, P. W. G.; Tatchell, A. R. *Vogel's Textbook of Practical Organic Chemistry*, 5th ed.; Pearson: Harlow, U.K., 1989.
- (12) Pachisia, S.; Gupta, R. Two Hg(II)-Based Macrocycles Offering Hydrogen Bonding Cavities: Influence of Cavity Structure on Heterogeneous Catalysis. *Cryst. Growth Des.* **2019**, *19*, 6039–6047.
- (13) *Smart & SAINT Software Reference Manuals*, version 6.45; Bruker Analytical X-ray Systems, Inc.: Madison, WI, 2003.
- (14) *CrysAlis CCD, RED*, version 1.711.13; Oxford Diffraction Poland Sp, 1995–2003.
- (15) Sheldrick, G. M. SHELXS-97, A short history of SHELX. *Acta Crystallogr., Sect. A: Found. Crystallogr.* **2008**, *A64*, 112–122.
- (16) SHELXL 2016-6; Sheldrick, G. M. *Acta Crystallogr.* **2015**, *C71*, 3–8.
- (17) (a) Brandenburg, K. DIAMOND; Crystal Impact GbR: Bonn, Germany, 1999. (b) Macrae, C. F.; Bruno, I. J.; Chisholm, J. A.; Edgington, P. R.; McCabe, P.; Pidcock, E.; Rodriguez-Monge, L.; Taylor, R.; van de Streek, J.; Wood, P. A. Mercury CSD 2.0 – New Features for the Visualization and Investigation of Crystal Structures. *J. Appl. Crystallogr.* **2008**, *41*, 466–470. (c) Dolomanov, O. V.; Bourhis, L. J.; Gildea, R. J.; Howard, J. A.; Puschmann, H. OLEX₂: a complete structure solution, refinement and analysis program. *J. Appl. Crystallogr.* **2009**, *42*, 339–341.
- (18) (a) Benson, R. E.; Ellis, C. A.; Lewis, C. E.; Tiekink, E. R. 3D-, 2D- and 1D-supramolecular structures of $\{\text{Zn}[\text{S}_2\text{CN}(\text{CH}_2\text{CH}_2\text{OH})\text{-R}]_2\}_2$ and their $\{\text{Zn}[\text{S}_2\text{CN}(\text{CH}_2\text{CH}_2\text{OH})\text{R}]_2\}_2$ (4, 4'-bipyridine) adducts for R = $\text{CH}_2\text{CH}_2\text{OH}$, Me or Et: polymorphism and pseudo-polymorphism. *CrystEngComm* **2007**, *9*, 930–940. (b) Almaraz, E.; Foley, W. S.; Denny, J. A.; Reibenspies, J. H.; Golden, M. L.; Darensbourg, M. Y. Development of Five-Coordinate Zinc Mono- and Dithiolates as S-Donor Metalloligands: Formation of a Zn–W Coordination Polymer. *Inorg. Chem.* **2009**, *48*, 5288–5295. (c) Zheng, A. X.; Si, J.; Tang, X. Y.; Miao, L. L.; Yu, M.; Hou, K. P.; Wang, F.; Li, H. X.; Lang, J. P. Reactions of the cationic zinc thiolate model complex $[\text{Zn}(\text{Tab})_4](\text{PF}_6)_2$ with N-donor ligands and cobalt dichloride. *Inorg. Chem.* **2012**, *51*, 10262–10273. (d) Fu, R.; Xiang, S.; Hu, S.; Wang, L.; Li, Y.; Huang, X.; Wu, X. Assembled bright green fluorescent zinc coordination polymer. *Chem. Commun.* **2005**, 42, 5292–5294.
- (19) (a) Singh, V.; Kumar, V.; Gupta, A. N.; Drew, M. G.; Singh, N. Effect of pyridyl substituents leading to the formation of green luminescent mercury(II) coordination polymers, zinc(II) dimers and a monomer. *New J. Chem.* **2014**, *38*, 3737–3748. (b) Yadav, C. L.;

Rajput, G.; Bisht, K. K.; Drew, M. G.; Singh, N. Spontaneous Resolution upon Crystallization and Preferential Induction of Chirality in a Discrete Tetrahedral Zinc(II) Complex Comprised of Achiral Precursors. *Inorg. Chem.* **2019**, *58*, 14449–14456.

(20) (a) Zukerman-Schpector, J.; Haiduc, I.; Tiekink, E. R. The metal–carbonyl $\cdots\pi$ (aryl) interaction as a supramolecular synthon for the stabilisation of transition metal carbonyl crystal structures. *Chem. Commun.* **2011**, *47*, 12682–12684. (b) Yeo, C. I.; Halim, S. N. A.; Ng, S. W.; Tan, S. L.; Zukerman-Schpector, J.; Ferreira, M. A.; Tiekink, E. R. Investigation of putative arene-C–H $\cdots\pi$ (quasi-chelate ring) interactions in copper(I) crystal structures. *Chem. Commun.* **2014**, *50*, 5984–5986.

(21) Li, G.; Song, Y.; Hou, H.; Li, L.; Fan, Y.; Zhu, Y.; Meng, X.; Mi, L. Synthesis, crystal structures, and third-order nonlinear optical properties of a series of ferrocenyl organometallics. *Inorg. Chem.* **2003**, *42*, 913–920.

(22) (a) Sharma, P.; Gupta, M.; Kant, R.; Gupta, V. K. One-pot synthesis of various 2-amino-4*H*-chromene derivatives using a highly active supported ionic liquid catalyst. *RSC Adv.* **2016**, *6*, 32052–32059. (b) Majumdar, N.; Paul, N. D.; Mandal, S.; de Bruin, B.; Wulff, W. D. Catalytic Synthesis of 2*H*-Chromenes. *ACS Catal.* **2015**, *5*, 2329–2366.